JOURNAL OF GEOPHYSICAL RESEARCH, VOL. 97, NO. C11, PAGES 17,905–17,924, NOVEMBER 15, 1992

Using the Extended Kalman Filter with a Multilayer Quasi-Geostrophic Ocean Model

GEIR EVENSEN

Nansen Environmental and Remote Sensing Center, Bergen, Norway

The formulation of the extended Kalman filter for a multilayer nonlinear quasi-geostrophic ocean circulation model is discussed. The nonlinearity in the ocean model leads to an approximative equation for error covariance propagation, where the transition matrix is dependent on the state trajectory. This nonlinearity complicates the dynamics of the error covariance propagation, and effects which are nonexistent in linear systems contribute significantly. The transition matrix can be split into two parts, where one part results in pure evolution of error covariances in the model velocity field, and the other part contains a statistical correction term caused by the nonlinearity in the model. This correction term leads to a linear unbounded instability, which is caused by the statistical linearization of the nonlinear error propagation equation. Different ways of handling this instability are discussed. Further, nonlinear small-scale instabilities also develop, since energy is accumulated at wavelengths $2\Delta x$, owing to the numerical discretization. These small-scale oscillations are removed with a Shapiro filter, and the effect they have on the error covariance propagation is discussed. Some data assimilation experiments are performed using the full extended Kalman filter, to examine the properties of the filter. An experiment where only the first part of the transition matrix is used to propagate the error covariances is also performed. This simplified experiment actually performs better than the full extended Kalman filter because the unbounded instability associated with the statistical correction term is avoided.

INTRODUCTION

The concept "data assimilation" denotes methods which combine dynamical models of a system with observations in order to improve the knowledge of the system. These methods are motivated by the following:

1. A mathematical model will never give an exact description of the state of a dynamical system. It will be subject to errors from estimated model parameters, neglected physics, solution techniques, forcing data, and errors in initial and boundary conditions. The model will therefore only give an approximate description of the physical processes as functions of space and time.

2. A set of measurements will never be complete. There will always be physics on some scales which are not resolved by the measurements, and they will only be available sparsely in space and time. A set of measurements is also subject to errors and will therefore only give an approximate description of the complete state as a function of space and time.

A data assimilation system should improve the estimate of a state by extracting a maximum amount of information from both the measurements and the dynamical model, and this information should be combined in an optimal way. The main objectives of a data assimilation system are to improve the forecasting capability, and to provide a sophisticated data analysis tool. It may be used to improve initial and boundary conditions, to estimate badly known model parameters and to improve error estimates. The measurements are interpolated consistently with the model dynamics, and more information is extracted from the data. The model is constrained by the measurements and will not drift away from the observed state.

Paper number 92JC01972.
0148–0227/93/92JC–01972$05.00

The importance of a reliable data assimilation system in oceanography is increasing, owing to the large amounts of oceanographic data which will be available in the future. It is mainly in the last decade that data assimilation has gained interest in the oceanographic community, although the method has been used in meteorology for some time.

There are mainly two general concepts which have been discussed for data assimilation. The "variational/adjoint" method has been the most used scheme [e.g. , *Lewis and Derber*, 1985; *Talagrand and Courtier*, 1987; *Courtier and Talagrand*, 1987; 1990; *Long and Thacker*, 1989*a*,*b*; *Thacker and Long*, 1988; *Thacker*, 1988]. Given a set of measurements distributed in a certain time interval, the initial conditions and unknown parameters for the model which are sought, are those resulting in the model trajectory that best fits the measurements in some sense. This can be formulated as a constrained minimization problem where the ocean model operates as a strong constraint on a cost function measuring the distance between the model solution and the measurements in a time interval. The cost function will normally include terms which ensure smoothness of the model solution, and it may also contain different weighting on different measurements. A drawback of the method is the difficulty of including model errors (system noise). This may result in bad solutions which depart significantly from the measurements, especially if the ocean model is unable to describe important phenomena which are contained in the measurements.

Another class of methods are those described as "sequential" data assimilation. Starting from some best guess initial condition, the model solution is sequentially updated in every time step where measurements are available. The model solution will, under certain conditions, approach the observed state. At the same time, it will propagate the previous information which has been assimilated forward in time to increase the knowledge of the system. This group of methods requires an updating scheme, which combines

the model solution and the measurements to find a better state estimate. "Better" normally means that the updated estimate is closer to the data then the previous estimate, and at the same time is smooth and physically acceptable. The methods of "direct insertion" and the "Kalman filter" represent the two extremes of updating schemes. Direct insertion means that the value from a measurement is directly inserted at the grid point corresponding to the location of the measurement. This may of course lead to spikes and discontinuities in the model solution. The Kalman filter [see, e.g. , *Gelb*, 1974] is the other extreme, where the update is based on information about the statistical properties of the errors in both the measurements and the model state, and therefore the error covariance matrices of both the state estimate and the measurements must be known. The Kalman filter gives the optimal linear update in a least squares sense, based on the known statistics. It also ensures a smooth update determined by the covariance functions describing the correlation of the errors between variables at different grid points. The full Kalman filter is extremely expensive to compute, both in number of numerical operations and storage. The propagation of the error covariance matrix requires an amount of computation, which is $2n$ times a pure ocean model integration, where n is the number of state variables. Further, the error covariance matrix of size $n \times n$ must be stored.

There is also a number of methods in between these two extrema, which try to generate smooth updates by using more or less ad hoc correlation or influence functions in different ways. An example is optimal interpolation (OI) which has been used by meteorologists for operational weather prediction. This method has recently been discussed in the context of a quasi-geostrophic model by *Rienecker and Miller* [1991] for oceanographic applications. In OI a constant error covariance matrix is used in the standard Kalman filter equations to update the state vector when measurements are available. It is not propagated forward in time, and this results in major computational savings. Although the information from dynamical propagation of error statistics is lost, this method may give good results and it should be considered, maybe in connection with the full Kalman filter, where results may be compared. An excellent review on data assimilation has been given by *Ghil and Malanotte-Rizzoli* [1991].

In a data assimilation system for mesoscale ocean circulation, there are some issues that should be considered. The ocean model must be able to describe the dominant physics in a realistic manner, which requires it to be nonlinear. For most applications, it should also contain both barotropic and baroclinic instabilities. Since the data assimilation methods for nonlinear dynamics are extremely complicated, the model should be as simple as possible. A second criteria is that a sophisticated error statistics scheme should be used. We believe that good estimates of the error statistics are necessary to provide reliable state estimates. The improvement of the state estimate at locations where measurements are assimilated, and also the advection of this information by the background velocity field, should be reflected when new measurements are assimilated.

In this paper the extended Kalman filter is used with a nonlinear multilayer quasi-geostrophic (QG) model. This provides us with both a realistic ocean model and a very sophisticated error statistics scheme. The extended Kalman filter is an extension of the common Kalman filter and may be used when the model dynamics or the measurement equation is nonlinear. It consists of an approximative equation for the propagation of error covariances, and also approximative filter equations if the measurement equation is nonlinear.

When changing from a linear system to nonlinear dynamics the possible existence of a wide variety of phenomena which are nonexistent in the linear theory is introduced. Nonlinear systems may have solutions with multiple equilibria, where the solutions sometimes abruptly undergo transitions from one equilibrium to another as parameters change (bifurcations). Also chaotic behavior occurs in many deterministic systems, where solutions exhibit an apparently random behavior. The *Lorenz* [1963] model is probably the best known example of chaotic systems. It has solutions which undergo "unpredictable" transitions between two different equilibria (chaos). As discussed by *Miller and Ghil* [1990], a sequential data assimilation scheme should handle these abrupt transitions caused by bifurcations and indicate the correct qualitative state of the system. Further, it should also provide reliable error estimates, reflecting possibly chaotic behavior in the system. The existence of such nonlinear phenomena in a QG model has been pointed out by *Chao* [1984].

In the following, some of the properties of the Kalman filter are discussed. A simple example, where the Kalman filter is used to assimilate synthetic measurements in a linear one-dimensional advection equation, is used to illustrate the Kalman filter. Then the ocean model is discussed, the equation for evolution of the error covariance matrix is derived, and the equations for the extended Kalman filter are given. The effects of nonlinearities are discussed and examples are included which illustrate the properties of the extended Kalman filter in a nonlinear QG model. Conclusions are given in the final section.

THE KALMAN FILTER

The Kalman filter has been derived in a number of books on control theory [e.g. , *Gelb*, 1974; *Jazwinski*, 1970; *Tzafestas*, 1978; *Bierman*, 1977; *Anderson*, 1979; *Stengel*, 1986]. In oceanography the Kalman filter has been used by *Budgell* [1986, 1987] to describe nonlinear and linear shallow water wave propagation in branched channels, using one-dimensional cross-sectionally integrated equations. *Miller*, [1986] used a one-dimensional linear barotropic QG model to investigate the properties of the Kalman filter. He also gave a derivation of the Kalman filter equations. In two more recent papers, *Miller and Cane* [1989] and *Miller* [1990] used the Kalman filter to assimilate wind data in a wind-driven numerical model of the equatorial Pacific. The physical model was the linearized equation of motion on an equatorial β plane. *Bennett and Budgell* [1987, 1989] have analyzed the Kalman filter and the Kalman smoother in connection with a spectral approximation for the barotropic potential vorticity equation in a doubly periodic domain. They studied the convergence of the Kalman filter in the limit of high numerical resolution. *Ghil* [1989] discussed the Kalman filter as a data assimilation method in oceanography, and used it with a simple linear barotropic model. The Kalman filter for use in meteorology has recently been discussed by *Cohn and Parrish* [1991], who discussed the propagation of error covariances in a two-dimensional linear model. *Dee*

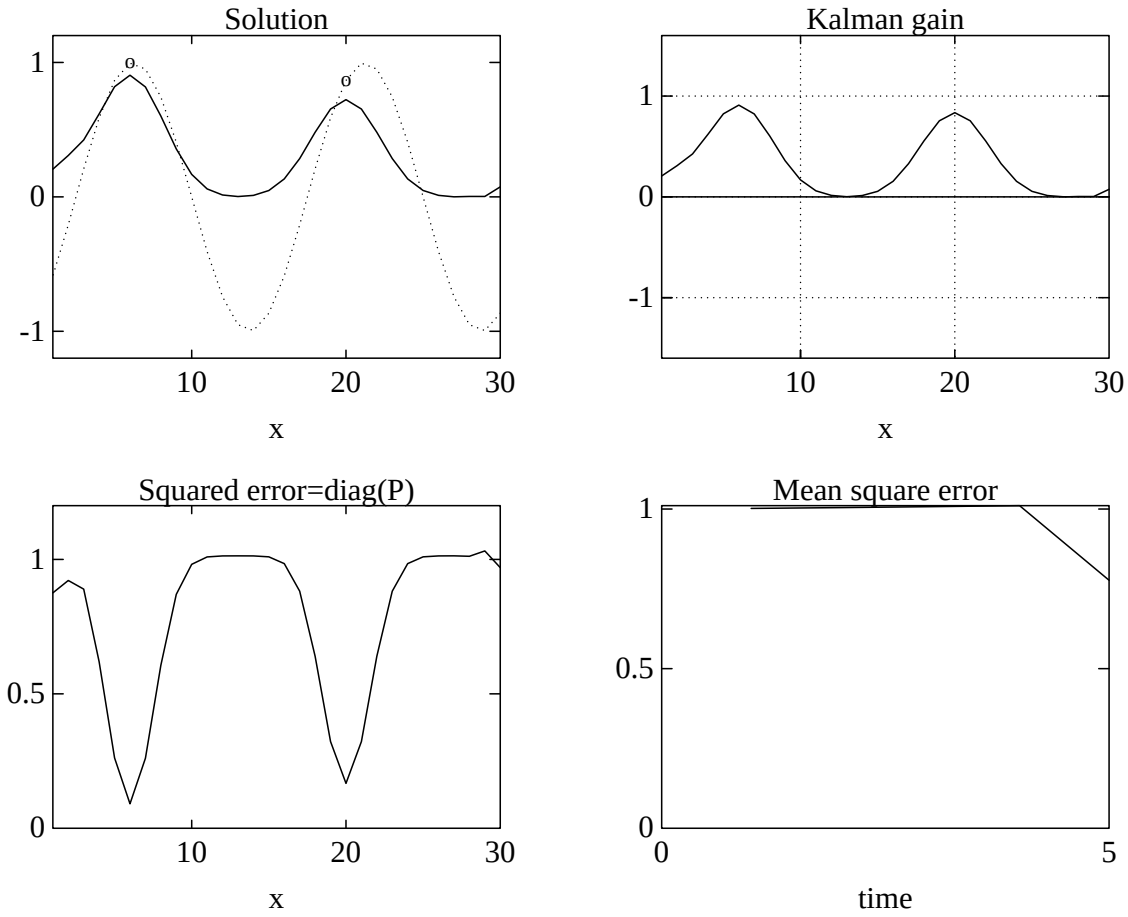

Fig. 1. Solution of the advection equation after one update with the Kalman filter. The upper left plot shows the true solution as a dotted line and the estimated solution as the solid line. The circles are the values of the measurements. The lower left plot shows the estimated error variance for each grid point (the diagonal elements of P). The Kalman gain influence (columns of K) are shown in the upper right plot. The lower right plot shows the time history of the mean square error, i.e. , the normalized trace of P.

[1991] has introduced a simplified and numerically more efficient method where the error covariances are propagated with simplified equations.

A complete derivation of the Kalman filter can be found in the literature described above. This paper concentrates on some of the properties of the filter. First of all, the filter is linear and it is also optimal in a least squares sense, and therefore no other linear filter exists which is better. It is assumed that a state estimate vector $\boldsymbol{\psi}_k \in \Re^n$ and a vector of measurements $\mathbf{z}_k \in \Re^{n_o}$ are given at time t_k, where n is the number of unknowns in the state vector and n_o is the number of measurements. The elements in an updated or analyzed state vector $\boldsymbol{\psi}_k^a$ are then given by a linear combination of all the elements in both the state estimate vector $\boldsymbol{\psi}_k$ and the measurement vector $\mathbf{z}_k$. This linear combination is determined so that the error in the update is minimized in a least squares sense.

A discretized linear model without forcing can be formulated as

$$\boldsymbol{\psi}_k^f = A\boldsymbol{\psi}_{k-1}^a, \tag{1}$$

where A is the advection operator between each time step. The superscripts f and a denote the forecasted and analyzed estimate, respectively. The underlying system evolves according to

$$\boldsymbol{\psi}_k^t = A\boldsymbol{\psi}_{k-1}^t + \mathbf{v}_k, \tag{2}$$

where $\boldsymbol{\psi}_k^t$ is the true state at t_k, and $\mathbf{v}_k$ contains the unbiased model system noise. The system noise takes account of errors in the mathematical model, the numerical approximation, and the boundary conditions. An error covariance matrix for the state vector $\boldsymbol{\psi}_k$ is defined as $P_k = \mathcal{E}[(\boldsymbol{\psi}_k - \mathcal{E}[\boldsymbol{\psi}_k])(\boldsymbol{\psi}_k - \mathcal{E}[\boldsymbol{\psi}_k])^T]$, where $\mathcal{E}[\,]$ means the expected value. An equation for the propagation of the error covariance matrix is derived from equation (2) as

$$P_k^f = AP_{k-1}^a A^T + Q_k, \tag{3}$$

where $Q_k = \mathcal{E}[\mathbf{v}_k\mathbf{v}_k^T] \in \Re^{n\times n}$ is the system error covariance matrix.

The measurement vector $\mathbf{z}_k$ is related to the true state vector through the measurement equation

$$\mathbf{z}_k = H_k\boldsymbol{\psi}_k^t + \mathbf{w}_k, \tag{4}$$

where $H_k \in \Re^{n_o\times n}$ is the measurement matrix and $\mathbf{w}_k$ is a vector containing unbiased measurement noise. All kinds of measurements which may be related to the state variable by the linear operator H_k can then be used. Measurements which are nonlinear functions of $\boldsymbol{\psi}_k$ can be treated in an approximative way by the extended Kalman filter. The op-

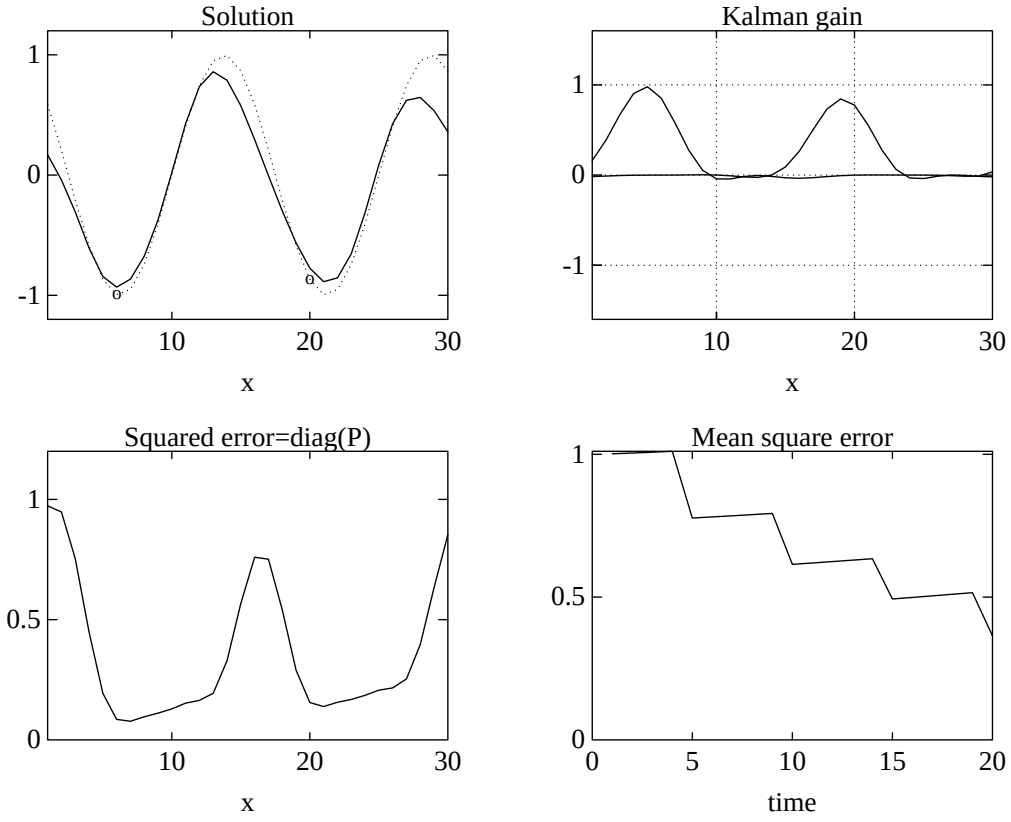

Fig. 2. The same as Figure 1 but after four updates with the Kalman filter.

timal estimate is

$$\boldsymbol{\psi}_k^{\mathrm{a}} = \boldsymbol{\psi}_k^{\mathrm{f}} + K_k(\mathbf{z}_k - H_k\boldsymbol{\psi}_k^{\mathrm{f}}), \tag{5}$$

where the Kalman gain or influence matrix $K_k \in \Re^{n\times n_\mathrm{o}}$ is given by

$$K_k = P_k^{\mathrm{f}} H_k^{\mathrm{T}}[H_k P_k^{\mathrm{f}} H_k^{\mathrm{T}} + R_k]^{-1}, \tag{6}$$

where $R_k = \mathcal{E}[\mathbf{w}_k\mathbf{w}_k^{\mathrm{T}}] \in \Re^{n_\mathrm{o}\times n_\mathrm{o}}$ is the measurement error covariance matrix. The Kalman gain matrix contains the influence from a measurement on the different elements of $\boldsymbol{\psi}_k$ in the columns of K_k, and it contains the influence on one element of $\boldsymbol{\psi}_k$ from all of the measurements in the rows of K_k.

In the case with only one measurement, and when this measurement is exactly observing an element of the state vector, the matrix H_k will reduce to a vector with zero at all elements except the one corresponding to the element ψ_k^{m} in $\boldsymbol{\psi}_k$ which is measured. The inverse matrix in the equation for the Kalman gain will then be a scalar which is the sum of the error variance to ψ_k^{m} and the measurement z_k. The product $P_k H_k^{\mathrm{T}}$ is a vector containing the error covariance function for ψ_k^{m}. The Kalman gain will therefore be equal to the error covariance function to ψ_k^{m} divided by the sum of the error variances of ψ_k^{m} and the measurement z_k. In the case when the measurement error is large, the influence of the measurement will be small. In the case when the measurement error is small the influence function will approach one, and the influence of the measurement becomes large.

When the filter is used to improve an estimate, the error is reduced and the error covariance matrix is updated according to the formula

$$P_k^{\mathrm{a}} = P_k^{\mathrm{f}} - H_k K_k P_k^{\mathrm{f}}. \tag{7}$$

Equations (5)–(7) constitute the Kalman filter update equations.

A Simple Example

To illustrate some of the properties of the Kalman filter, a simple case with a linear one-dimensional advection equation

$$\frac{\partial \Psi}{\partial t} + c\frac{\partial \Psi}{\partial x} = 0 \tag{8}$$

is discussed. This equation describes pure advection of the quantity Ψ with constant velocity c, without distortion of the shape or amplitude of Ψ. When discretized with a one-step numerical scheme in time, this equation may be written on the form (1), and it has an error covariance propagation equation given by (3).

A study of a simple linear system used for illustrational purposes has also been given by *Ghil et al.* [1981]. They discussed a simplified linear barotrophic model for one-dimensional atmospheric wave propagation, where a modified Kalman filter, designed to remove fast wave modes, was compared to the standard Kalman filter. The time evolution and propagation of averaged errors in data-rich areas (land), and in data-sparse areas (ocean) were discussed together with influence functions at different locations. Here a simpler one-dimensional advection equation has been used, and spatial maps of the error variances have been included, in addition to influence functions and time evolution of average errors.

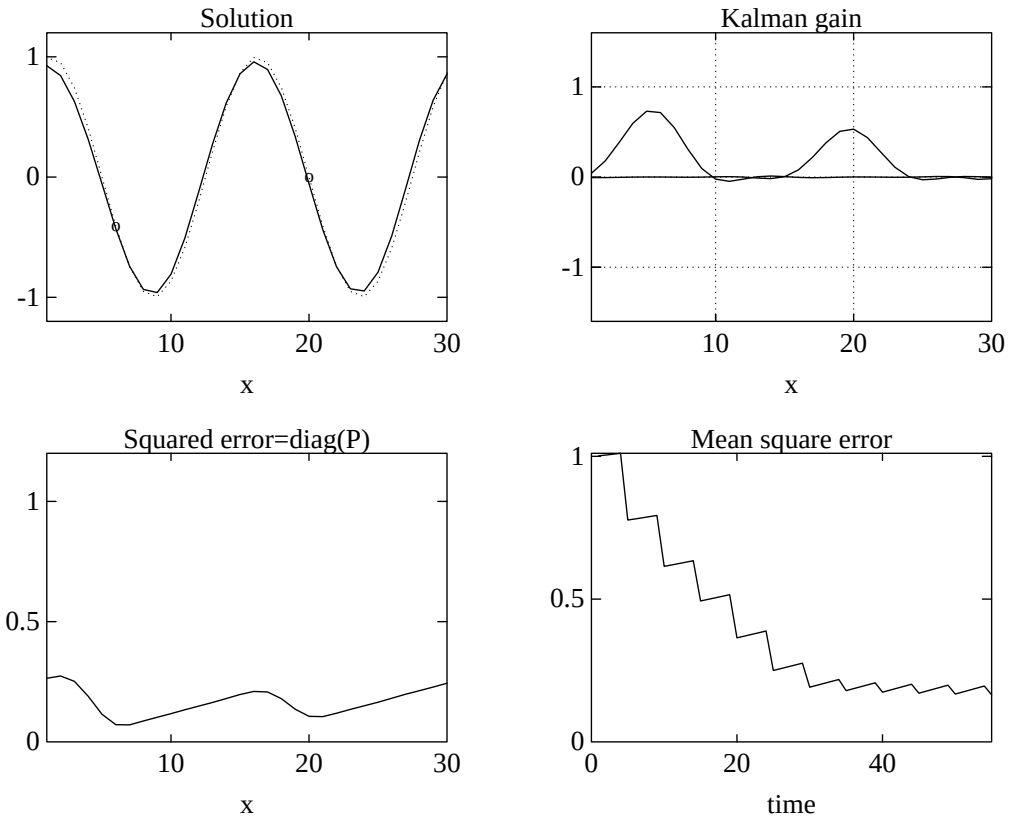

Fig. 3. The same as Figure 1 but after 11 updates with the Kalman filter.

As a test case for the advection equation, a periodic domain is used, where a sinusoidal wave, traveling from left to right (i.e. , $c > 0$), with wavelength equal to half the length of the domain is given as exact solution of the equation. Values of this solution at two locations $x = 5$ and $x = 20$ are taken as measurements. It is assumed that no initial information about the solution is available, and the integration starts with the amplitude of the initial wave equal to zero. The initial error variance is also set equal to one and a correlation function of the form $\exp\left\{-(r/r_c)^2\right\}$ is assumed, where r is the distance between grid points and r_c is the e-folding scale of the correlation function. The solution is propagated with equation (8), and at every fifth time step the solution is updated with the two measurements from the reference solution. Even though the measurements are perfect, a certain error variance is assumed to decrease their influence. The measurement at $x = 20$, has twice as high error variance as the measurement at $x = 5$.

Figure 1 shows the solutions after one filter update. The upper left plot displays the estimate of the correct solution as given by the Kalman filter (solid line), and the correct solution which is estimated as the dotted line. The upper right plot shows the two columns of the Kalman gain matrix K_k which describe the influence from the measurements on the estimate. Note the difference in amplitude of the influence functions for the two measurements. The width of these functions is directly connected to the cross correlation between off diagonal elements in the error covariance matrix P_k. This ensures a spatially smooth update, and a measurement will normally have influence on a domain of a few characteristic lengths of the system, determined by the error covariance function. In the lower left plot the diagonal of P_k is plotted, where each element contains the square of the error (variance), for the state vector. After an update, the error is reduced in a spatial domain around the locations of the measurements. The lower right plot shows the trace of P_k divided by the number of grid points, i.e. , the mean square error, as a function of time.

Figure 2 shows the solutions after four filter updates, i.e. 20 time steps. The estimated solution is now approaching the form and amplitude of the exact reference solution. The errors have decreased further, and note that the information gained at the measurement locations has propagated with velocity c, and the errors downstream of each measurement point are therefore smaller than upstream. The average error is decreasing each time measurements are used to improve the estimate. Between the updates, the average error is slightly increasing due to the system noise Q_k, which is added every time step.

Figure 3 shows the solutions after 11 filter updates. The filter has now reached a state where the error increase between measurement updates is matched by the error reduction caused by the assimilation of measurements. The solution is very close to the reference solution and the errors are oscillating between a minima right after measurement updates, and a maxima right before measurement updates. Because of the system noise, the errors will always increase unless information is provided by measurements. The amplitudes of the Kalman gain functions have decreased, since the errors in the model state have decreased, and the model predicted estimate is weighted more strongly.

Similar results were also found by *Miller* [1986] using a one-dimensional linear barotropic QG model.

EQUATIONS FOR THE LAYERED MODEL

The ocean model is multilayered and describes conservation of potential vorticity ζ_l (hereafter called just "vorticity") in each layer on an f plane. The mean layer thicknesses are D_l, and the density in each layer is ρ_l, where l denotes layer number; $l = 1$ in the upper layer. Ψ_l is the stream function in layer l. The horizontal length scale R_d is the internal Rossby radius of deformation of the upper layer, given by $R_\mathrm{d}^2 = \{(\rho_2 - \rho_1) g D_1\} / \{\rho_0 f^2\}$, where g is the gravitational acceleration, ρ_0 is averaged density and f is the Coriolis parameter. The characteristic horizontal velocity is denoted U, yielding a time scale $T = R_\mathrm{d}/U$. The pressure scale is $\rho_0 f U R_\mathrm{d}$, and the stream function scale is $U R_\mathrm{d}$. The nondimensional quasi-geostrophic equations [see *Pedlosky*, 1987] are

$$(\frac{\partial}{\partial t} + u_l \frac{\partial}{\partial x} + v_l \frac{\partial}{\partial y})\zeta_l = 0, \quad l = 1, n_z, \tag{9}$$

where n_z is the number of layers and the velocities are the geostrophic approximations

$$u_l = -\frac{\partial \Psi_l}{\partial y} \qquad v_l = \frac{\partial \Psi_l}{\partial x}. \tag{10}$$

The vorticity in each layer is given by

$$\zeta_1 = \nabla^2 \Psi_1 + fr_{1,2}(\Psi_2 - \Psi_1), \tag{11a}$$

$$\zeta_l = \nabla^2 \Psi_l - fr_{l,1}(\Psi_l - \Psi_{l-1}) + fr_{l,2}(\Psi_{l+1} - \Psi_l), \text{ for } l = 2, n_z - 1, \tag{11b}$$

$$\zeta_{n_z} = \nabla^2 \Psi_{n_z} - fr_{n_z,1}(\Psi_{n_z} - \Psi_{n_z-1}) + \eta, \tag{11c}$$

which constitutes a set of Helmholtz equations for Ψ when ζ is known. The Laplacian is $\nabla^2 = \partial^2/\partial^2 x + \partial^2/\partial^2 y$, and the constants $fr_{l,1}$ and $fr_{l,2}$ are "nondimensional Froude numbers"

$$fr_{l,1} = \frac{D_1}{D_l} \frac{\rho_2 - \rho_1}{\rho_l - \rho_{l-1}} \tag{12}$$

and

$$fr_{l,2} = \frac{D_1}{D_l} \frac{\rho_2 - \rho_1}{\rho_{l+1} - \rho_l}. \tag{13}$$

The bottom topography term is

$$\eta = \varepsilon^{-1} \frac{h}{D_{n_z}}, \tag{14}$$

with ε as the Rossby number and h as bottom topography. These equations have been used extensively for mesoscale ocean modeling by, among others, *Ikeda* [1981], *Ikeda and Apel* [1981], *Ikeda et al.* [1989], and *Haugan et al.* [1991]. The reason for using this model instead of a more complex primitive equation model, is the simple dynamics of the model. It describes conservation of vorticity in each layer, and the only physics included are relative vorticity (∇^2 term), stretching or compression of a vorticity column and topographical influence in addition to barotropic and baroclinic instabilities. This leads to solutions which are relatively simple to interpret, and the model may be characterized as the simplest circulation model which is able to give a "realistic" representation of mesoscale variability in the ocean. It has only one dependent variable for each grid point, and this limits the size of the matrices used in the Kalman filter.

The model constitutes a well formulated problem when boundary conditions are specified as proposed by *Charney et al.* [1950], i.e. , the stream function is specified at all boundary points and the vorticity is specified at inflow boundaries. Some restrictions to the well posedness occur when the flow is parallel to the boundary as pointed out by, among others, *Miller and Bennett* [1988].

DISCRETIZATION

The stream function is chosen as the state variable. If the vorticity was used, the transition matrix would be rather complicated to compute. Measurements are also normally given in terms of sea-level or velocities, which are hard to convert to vorticity information. The stream function Ψ is discretized on a uniform grid of dimension $n_x \times n_y$ in n_z layers, and stored in the vector $\boldsymbol{\psi}_k \in \Re^n$ in some convenient order, where $n = n_z n_x n_y$ is the total number of grid points. Hereafter the vectors $\boldsymbol{\psi}_k$ and $\boldsymbol{\zeta}_k$ of dimension n denote the stream function and the potential vorticity, respectively, at time $t = t_k$. When starting with the stream function $\boldsymbol{\psi}_k$, the solution algorithm for the model equations is as follows:

1. Calculate the vorticity $\boldsymbol{\zeta}_k$ at all internal grid points from the equations (11) by using a five-point second-order finite difference formula for the horizontal Laplacian operator ∇^2. To be able to use the same advection scheme for all internal grid points, a simple scheme is used to estimate the vorticity at the boundaries. The accuracy of this scheme is not important when closed boundaries are used, as is the case in this paper.

2. Advect the vorticity at the internal grid points according to equation (9) with velocities calculated from the stream function according to equation (10).

3. Apply appropriate boundary conditions for the stream function at time t_{k+1}, and solve the system of Helmholtz equations (11) to find the stream function at time t_{k+1}.

For an advection scheme which is one step in time, the equation for the stream function at time t_{k+1} may be written as

$$L' \boldsymbol{\psi}_{k+1} + \boldsymbol{\eta}' = \Gamma(\boldsymbol{\psi}_k)(L'' \boldsymbol{\psi}_k + \boldsymbol{\eta}). \tag{15}$$

$L' \in \Re^{n_\mathrm{i} \times n}$ is the operator resulting from the discretized Laplacian plus the coupling terms between the layers in the system of Helmholtz equations (11), n_i is the number of internal grid points; $n_\mathrm{i} = n_z(n_x - 2)(n_y - 2)$; $\boldsymbol{\eta}' \in \Re^{n_\mathrm{i}}$ is the bottom topography at all internal grid points; and $\boldsymbol{\eta} \in \Re^n$ contains the bottom topography at all internal grid points and zero elements at the boundary points. The matrix L'' is the same as L' except that L'' includes extra rows for the estimation of boundary vorticity. $\Gamma(\boldsymbol{\psi}_k) \in \Re^{n_\mathrm{i} \times n}$ is the advection matrix which updates the vorticity at all the internal grid points. Equation (15) is then a system of n_i linear equations for n unknowns and it can not be solved uniquely for $\boldsymbol{\psi}_{k+1}$ without additional $n - n_\mathrm{i}$ equations to close the system. These additional equations are the boundary conditions for the stream function, and they can be formulated as

$$I' \boldsymbol{\psi}_{k+1} = C_\mathrm{b} \boldsymbol{\psi}_k, \tag{16}$$

where $I', C_\mathrm{b} \in \Re^{(n - n_\mathrm{i}) \times n}$. The matrix I', when operating on $\boldsymbol{\psi}_{k+1}$ results in a vector containing the boundary stream function at t_{k+1}. The matrix C_b relates the value of the stream function at the boundaries to the stream function from the last time step.

The stream function on open boundaries may be kept constant in time, or it may be determined from a radiation condition. On closed boundaries the stream function will normally be constant in time. If a linear and explicit scheme for the radiation condition is assumed, the equations for the boundary stream function can be contained in the rows of C_b corresponding to the different boundary points.

By using the boundary conditions (16) in equation (15), and by moving $\boldsymbol{\eta}'$ to the right-hand side, a system of linearly independent equations which have a unique solution for $\boldsymbol{\psi}_{k+1}$ results. The n_i vector function

$$\mathbf{f}'(\boldsymbol{\psi}_k) = \Gamma(\boldsymbol{\psi}_k)(L''\boldsymbol{\psi}_k + \boldsymbol{\eta}) \tag{17}$$

which contains the vorticity at all internal grid points, is defined. Further the n vector function $\mathbf{f}(\boldsymbol{\psi}_k)$ is defined, which includes $\mathbf{f}'(\boldsymbol{\psi}_k) - \boldsymbol{\eta}'$ at locations corresponding to internal grid points and the boundary conditions (16) for $\boldsymbol{\psi}_{k+1}$ at locations corresponding to boundary points. A compact matrix equation for the ocean model is

$$L\boldsymbol{\psi}_{k+1} = \mathbf{f}(\boldsymbol{\psi}_k), \tag{18}$$

where L contains the Helmholtz operator at rows corresponding to internal grid points, and one on the diagonal at elements corresponding to boundary points.

To advance the ocean model in time, a numerical advection scheme must be specified for stepping the vorticity field forward in time. This scheme is discussed in the appendix. A linear equation solver must be used to update the stream function from the system of Helmholtz equations (18). A block cyclic reduction algorithm which is based on the methods discussed by *Sweet* [1977], is developed and adapted to the matrices resulting from the coupled systems of Helmholtz equations (11). It can be used for rectangular grids of arbitrary size and dimension. This solver will be discussed in a forthcoming paper on the numerical implementation of the extended Kalman filter. Next the complete system of equations which constitutes the implemented data assimilation method is discussed.

PROPAGATION OF ERRORS

The numerical model (15) and (16) is purely deterministic. The initial, boundary, and governing equations are assumed to be known with certainty. However, initial and boundary conditions are never exactly known. The numerical model contains errors due to neglected physics and estimated parameters, and also due to numerical approximation and truncation errors. These errors can be included in the model as follows:

$$L'\boldsymbol{\psi}_{k+1} + \boldsymbol{\eta}' = \mathbf{f}'(\boldsymbol{\psi}_k) - L'\mathbf{v}^\mathrm{i}_{k+1}, \tag{19}$$

and

$$I'\boldsymbol{\psi}_{k+1} = C_\mathrm{b}\boldsymbol{\psi}_k + \mathbf{v}^\mathrm{b}_{k+1}, \tag{20}$$

where the vectors $\mathbf{v}^\mathrm{i}$ and $\mathbf{v}^\mathrm{b}$ contain unbiased noise due to all errors in the model equations, added to the state vector during a time step.

Taking the expectation of the equations (19) and (20) results in equations for propagation of the expected value $\mathcal{E}[\boldsymbol{\psi}]$,

$$L'\mathcal{E}[\boldsymbol{\psi}_{k+1}] + \boldsymbol{\eta}' = \mathcal{E}[\mathbf{f}'(\boldsymbol{\psi}_k)], \tag{21}$$

and

$$I'\mathcal{E}[\boldsymbol{\psi}_{k+1}] = C_\mathrm{b}\mathcal{E}[\boldsymbol{\psi}_k]. \tag{22}$$

Expanding the nonlinear function $\mathbf{f}'(\boldsymbol{\psi}_k)$ about $\mathcal{E}[\boldsymbol{\psi}_k]$ yields

$$\mathbf{f}'(\boldsymbol{\psi}_k) = \mathbf{f}'(\mathcal{E}[\boldsymbol{\psi}_k]) + \left.\frac{\partial \mathbf{f}'(\boldsymbol{\psi})}{\partial \boldsymbol{\psi}}\right|_{\boldsymbol{\psi}=\mathcal{E}[\boldsymbol{\psi}_k]} (\boldsymbol{\psi}_k - \mathcal{E}[\boldsymbol{\psi}_k]) + \cdots. \tag{23}$$

Taking the expectation of the expansion (23) gives

$$\mathcal{E}[\mathbf{f}'(\boldsymbol{\psi}_k)] = \mathbf{f}'(\mathcal{E}[\boldsymbol{\psi}_k]) + 0 + \cdots. \tag{24}$$

When substituting the expansion (23) into equation (19) and the expansion (24) into equation (21), and subtracting (21) from (19), an approximative equation for the propagation of errors for the internal grid points is found,

$$L'(\boldsymbol{\psi}_{k+1} - \mathcal{E}[\boldsymbol{\psi}_{k+1}]) = F'_k(\boldsymbol{\psi}_k - \mathcal{E}[\boldsymbol{\psi}_k]) - L'\mathbf{v}^\mathrm{i}_{k+1}, \tag{25}$$

where

$$F'_k = \left.\frac{\partial\, \Gamma(\boldsymbol{\psi})(L''\boldsymbol{\psi} + \boldsymbol{\eta})}{\partial \boldsymbol{\psi}}\right|_{\boldsymbol{\psi}=\mathcal{E}[\boldsymbol{\psi}_k]}. \tag{26}$$

A similar equation can be found for the boundary points as

$$I'(\boldsymbol{\psi}_{k+1} - \mathcal{E}[\boldsymbol{\psi}_{k+1}]) = C_\mathrm{b}(\boldsymbol{\psi}_k - \mathcal{E}[\boldsymbol{\psi}_k]) + \mathbf{v}^\mathrm{b}_{k+1}. \tag{27}$$

By inserting these equations into appropriate locations in the error propagation equation for the internal grid points (25), an approximative equation for the propagation of the error covariance matrix $P = \mathcal{E}[(\boldsymbol{\psi} - \mathcal{E}[\boldsymbol{\psi}])(\boldsymbol{\psi} - \mathcal{E}[\boldsymbol{\psi}])^\mathrm{T}]$ is found to be

$$LP_{k+1}L^T = F_k P_k F_k^\mathrm{T} + LQ_{k+1}L^\mathrm{T}, \tag{28}$$

where F_k is the transition matrix which contains the rows of F'_k for the internal grid points and the rows of C_b for the boundary points. Note the difference between this equation and the error propagation equation for the linear advection equation (3). Here the transition matrix F_k is a linearized approximate function of the state estimate. We also have to solve $2n$ elliptic systems to step the error covariance matrix forward in time.

For linear systems, the propagation of the error covariance is described by the linear dynamical model without reference to higher moments. In an optimal nonlinear filter the inclusion of an infinite number of equations for the moments, is required. The extended Kalman filter results from neglecting all moments of third and higher order. It has been proven to give good results in the extensive engineering literature (some of which is referenced above), and also in *Budgell* [1986] for oceanographic applications and *Lacarra and Talagrand* [1988] in meteorology, when the advective nonlinearity is not combined with too strong instability.

EQUATIONS FOR THE EXTENDED KALMAN FILTER

Now the complete set of equations which describes the extended Kalman filter for the QG model is discussed. When the superscript a denotes the analyzed estimate, f the forecasted estimate, and t the true state, the following equations constitute the extended Kalman filter for the QG model: The nonlinear equation for the propagation of the state estimate

$$L\boldsymbol{\psi}^\mathrm{f}_k = \mathbf{f}(\boldsymbol{\psi}^\mathrm{a}_{k-1}). \tag{29}$$

TABLE 1. Matrices and Vectors

	Dimension	Definition
$\boldsymbol{\psi}_k$	$\Re^n$	State vector
L	$\Re^{n\times n}$	Elliptic operator
$\mathbf{f}_k$	$\Re^n$	RHS in discretized model
$\mathbf{v}_k$	$\Re^n$	System noise
F_k	$\Re^{n\times n}$	Transition matrix
Q_k	$\Re^{n\times n}$	Model error covariance matrix
P_k	$\Re^{n\times n}$	State error covariance matrix
K_k	$\Re^{n\times n_o}$	Kalman gain matrix
H_k	$\Re^{n_o\times n}$	Measurement matrix
$\mathbf{z}_k$	$\Re^{n_o}$	Measurement vector
$\mathbf{w}_k$	$\Re^{n_o}$	Measurement noise
R_k	$\Re^{n_o\times n_o}$	Measurement error covariance matrix

The matrices and the vectors in the equations for the extended Kalman filter.

The equation for propagation of the error covariance matrix

$$LP_k^{\mathrm{f}}L^T = F_{k-1}P_{k-1}^{\mathrm{a}}F_{k-1}^{\mathrm{T}} + LQ_kL^{\mathrm{T}}. \tag{30}$$

The measurement equation which describes how measurements are related to the true state vector

$$\mathbf{z}_k = H_k\boldsymbol{\psi}_k^{\mathrm{t}} + \mathbf{w}_k. \tag{31}$$

The Kalman gain matrix gives the influence of the measurements on the state vector during a filter update,

$$K_k = P_k^{\mathrm{f}}H_k^{\mathrm{T}}[H_kP_k^{\mathrm{f}}H_k^{\mathrm{T}} + R_k]^{-1}. \tag{32}$$

The analyzed estimate,

$$\boldsymbol{\psi}_k^{\mathrm{a}} = \boldsymbol{\psi}_k^{\mathrm{f}} + K_k[\mathbf{z}_k - H_k\boldsymbol{\psi}_k^{\mathrm{f}}]. \tag{33}$$

The analyzed error covariance matrix,

$$\begin{aligned} P_k^{\mathrm{a}} &= [I - K_kH_k]P_k^{\mathrm{f}} \\ &= [I - K_kH_k]P_k^{\mathrm{f}}[I - K_kH_k]^{\mathrm{T}} + K_kR_kK_k^{\mathrm{T}}. \end{aligned} \tag{34}$$

The last expression in equation (34) should be used for numerical stability since the first expression contains the difference between two positive definite matrices, which may become nondefinite, but the last expression is a sum of two positive definite matrices. This is especially important in regions with low variance, which may become negative due to numerical errors. The vectors and matrices in the equations are listed in Table 1.

The main numerical tasks in solving these equations are the matrix multiplications and the elliptic systems which must be solved during each time step in order to propagate the error covariance. The storage of the full error covariance matrix P_k also limits the size of the problem to be solved. Note that the same elliptic solver can be used both for the ocean model and for the propagation of error covariances.

For the examples in this paper only closed boundaries has been used. This is satisfactory since the purpose of the paper is to give a general discussion of the formulation and the properties of the extended Kalman filter with a nonlinear QG model. The inclusion of open boundary conditions significantly complicates the boundary treatment, both for the ocean model and the error covariance propagation equation. A discussion of a more general boundary treatment will therefore be given in a forthcoming paper. By using closed boundary conditions the problem is well posed both for the ocean model and the error covariance propagation equation and no special problems occur.

EFFECTS OF NONLINEARITIES ON ERROR PROPAGATION

With a nonlinear model the dynamics of the error covariance propagation becomes much more complicated than what it would be if the model was linear. In general, very little can be said about the properties of a nonlinear filter, and every special case must be studied separately. The QG model results in equations with "modest" nonlinearity, since the only nonlinearity occurs on the right-hand side of the equation. It is not necessary to solve extra systems of equations resulting from a linearized nonlinear left-hand side, as was done in *Budgell* [1986].

The transition matrix for the internal grid points, (26) may be separated into two matrices. When the derivative is evaluated, it may be written as

$$F_k' = \Gamma(\mathcal{E}[\boldsymbol{\psi}_k])L'' + \left.\frac{\partial\Gamma(\boldsymbol{\psi})}{\partial\boldsymbol{\psi}}\right|_{\boldsymbol{\psi}=\mathcal{E}[\boldsymbol{\psi}_k]}(L''\mathcal{E}[\boldsymbol{\psi}_k] + \boldsymbol{\eta}). \tag{35}$$

The first term describes pure evolution of error covariances according to the model velocity field, where the velocity field is calculated from the model predicted state estimate. The second part includes the additional effect resulting from the error caused by evaluating the transition matrix as a function of the model predicted estimate instead of using the exact stream function. In a linear problem the second part is avoided since the transition matrix is independent of the model solution, and the first part will therefore exactly describe the evolution of error covariances. The second term contains the derivatives of the advection operator with respect to the stream function field, multiplied with the vorticity, and it is responsible for some important effects discussed below.

In a nonlinear numerical model, small-scale oscillations will occur in the solutions since energy is transferred between wave modes at different wave numbers. Energy is accumulated at waves with wavelength $2\Delta x$, which is the shortest wavelength resolved by the grid. This energy must be removed to avoid nonphysical small-scale instabilities in the solutions, and this is normally done by using a Shapiro filter of some order (see the appendix). When the extended Kalman filter is used to propagate error covariances, these instabilities will be important for two reasons. First, the transition matrix is directly dependent on the vorticity field through the second term in (35), and since the small-scale noise in the stream function is actually amplified in the vorticity field, this has strong effects on the error propagation. Secondly, since the same "advection" scheme is used for the propagation of error covariances as for advection of the model solution, small-scale instabilities will be created also in the error covariances by the first part of equation (35). This noise must be removed in both the model solution and the error covariance functions. Actually, if the model solution is filtered by the Shapiro filter [*Shapiro*, 1970], which is a linear operator, formulated as

$$\boldsymbol{\psi}_k^{\mathrm{filt}} = S\boldsymbol{\psi}_k, \tag{36}$$

the error covariance matrix should be updated according to

$$P_k^{\mathrm{filt}} = SP_kS^{\mathrm{T}}, \tag{37}$$

which is derived in the same way as the error covariance

propagation equation (28). The effect of adding these two equations to the total data assimilation system is illustrated in the next section.

The bottom topography term is not included in the first part of the error covariance propagation. It will only work through the nonlinear correction term where it gives a contribution to the potential vorticity. This would also be the case for a β term if it was included in the model. This means that the bottom topography can give a contribution to the error covariance propagation through the second term even if the model velocity field is zero. Occurrence of such an effect can be illustrated in the following way: Suppose there are errors of some level in the state vector. This will lead to an incorrect advection matrix, which in this case assumes zero velocity field. The second term therefore "corrects" for this error based on the statistical knowledge of the system.

DATA ASSIMILATION EXPERIMENT

Now a few cases which illustrate the use of the extended Kalman filter in the nonlinear QG model are discussed. The examples are chosen to illustrate the nonlinear effects on the error covariance propagation as well as the data assimilation process itself.

Parameters in the Ocean Model

For all the examples below, closed boundary conditions on a square 17×17 grid in two layers have been used. The internal Rossby radius is 5835 m, and the nondimensional grid spacing is $\Delta x = 0.5$. The velocity scale $U = 0.3$ m s^{-1}, and the initial condition in the reference case has a maximum nondimensional velocity equal to 1. The nondimensional time step is calculated from the CFL condition; typically $\Delta t = 0.5$. The total depth is 300.0 m and an upper layer of 50.0 m and a lower layer of 250.0 m have been used with a density difference of $\Delta\rho = 1.0$ kg m^{-3}. This results in Froude numbers $fr_{1,2} = 1.0$ and $fr_{2,1} = 0.2$, and the Rossby number U/fR_{d} becomes approximately 0.5. These parameters are typical for mesoscale processes in the Norwegian coastal waters. The QG model has proven to give good results in this parameter regime as discussed in [*Haugan et al.*, 1991; *Ikeda et al.*, 1989] even though the Rossby number is quite large.

Initial State Noise

As has been mentioned above, the Kalman filter requires knowledge of the error statistics to give reliable results. It is likely that the choice of a correct initial error covariance field is not crucial, at least for a dissipative system as is discussed here. After some time the error covariance matrix will be mostly determined by the information which is previously assimilated according to measurement updates, the addition of system noise, and the error covariance propagation. A bad choice of the initial error covariance matrix will influence the first data sets which are assimilated, by using incorrect influence from the data on the surrounding stream function values.

In many cases special knowledge of the solution is available, e.g. , at a closed boundary where the stream function can be chosen as constant in time [see *Holland*, 1978]. The measurements should not generate a significant inflow or outflow through a boundary which is actually closed, and this information must be included in the initial error field. By choosing both the initial and the system error variance to be zero at the closed boundaries, the influence from measurements taken inside the domain on these boundaries is avoided. The boundary stream function is then kept constant during the update in equation (33). However, for numerical stability a finite but low error variance should be used. With zero variance in a point, numerical truncation errors can result in negative variance at that point, and the error covariance matrix becomes nondefinite. The initial error field is defined for each of the grid points (i, j) from the function

$$E(i,j) = E_{\max} - (E_{\max} - E_{\min}) \exp\left(-d_{\mathrm{cb}}^2\right), \qquad (38)$$

where $E_{\min}$ has been chosen as a small number at the closed boundaries where the error should be zero, to ensure numerical stability. As long as $E_{\min}$ is small enough, this will not influence the solutions significantly. $E_{\max}$ is a maximum error which is approached in the center of the grid, and d_{cb} is the distance to the nearest boundary. The initial error covariance field is now calculated according to the formula

$$\sigma(l_1,i_1,j_1,l_2,i_2,j_2)^2 = E(i_1,j_1)E(i_2,j_2) \times \exp\left(-\frac{||\mathbf{r}_2 - \mathbf{r}_1||_2^2}{r_{\mathrm{h}}^2}\right) \exp\left(-(l_1-l_2)^2 r_{\mathrm{v}}^2\right) \qquad (39)$$

where the subscripts 1 and 2 are used to distinguish between the grid points to which the covariance is calculated. The $||\mathbf{r}_2 - \mathbf{r}_1||_2$ is the horizontal distance between the grid points, r_{h} is the horizontal correlation scale, l_1 and l_2 denote the layers for the two points, and r_{v} is a vertical correlation factor between the layers. The horizontal and vertical correlation scales have been chosen as $r_{\mathrm{h}} = 1.75$ and $r_{\mathrm{v}} = 0.7$ in all the following cases.

System Noise

In this paper no attempt has been made to estimate the correct system noise for the model. Here the same correlation function which is used for the initial noise above, and with the same horizontal and vertical scales, but with different values for $E_{\max}$ and $E_{\min}$ has been used. There may of course exist other choices which give better results, but an elaborate discussion on the subject will not be given here.

Pure Error Propagation

As has been discussed, the transition matrix F_k' as defined in equation (35) contains one part which describes pure evolution due to the model velocity field, and another part which contains a statistical correction caused by the nonlinearity. It is of interest to examine the effect and the importance of this nonlinear correction term. This can be done using a steady state stream function field. The velocity field will then be constant in time and so will the transition matrix, although both the velocity field and the transition matrix are still determined from the reference stream function. Since the velocity field is time independent, this case may be described by a linear model. This linear model will have a transition matrix equal to the first part of (35), with the nonlinear correction equal to zero. Note that when neglecting the second term of the transition matrix (35), the vorticity of the covariance functions is advected like a passive quantity in the model velocity field. It will then be possible to examine the effect of the second term in a con-

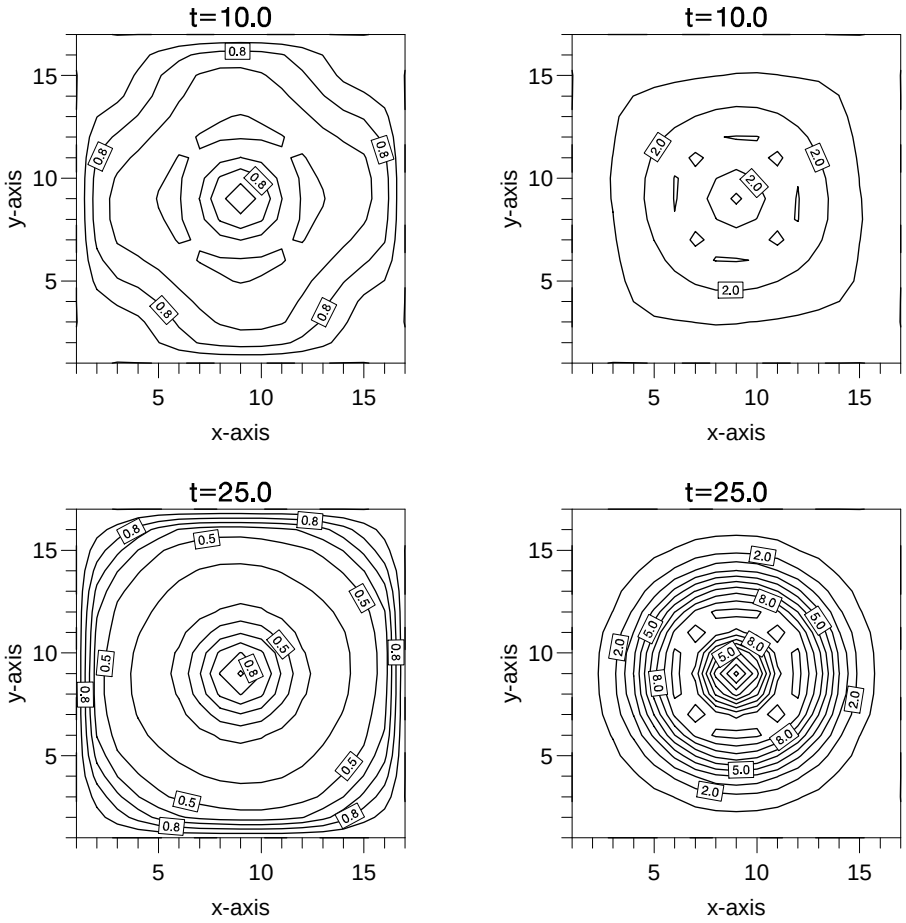

Fig. 4. Error variances in layer one for case 1A (left column) and case 1B (right column). For case 1A we have used contour intervals of 0.1, and for case 1B we have used contour intervals of 1.0.

sistent way. The following two cases will be discussed:

Case 1A: Steady barotropic eddy, using only the first part of the transition matrix (35) for error covariance propagation.

Case 1B: Steady barotropic eddy, using the full transition matrix (35) for error covariance propagation.

A steady barotropic anticyclonic eddy on a flat bottom is used. This stream function is also used as the initial condition in the reference case for the data assimilation experiments to be discussed next, and it is shown in Figure 8 for $t = 0.0$. In the left and right column of Figure 4 the evolution of the error variance field in cases 1A and 1B are shown, respectively. The initial error variance field has been set to one over the entire domain to clearly illustrate the effect of the velocity field on the error variance evolution. No system noise has been added.

In case 1A, the error variance field would stay constant in time if the error covariance propagation were described by exact numerical equations. It turns out that the error variance is fairly constant at the locations where the fluid velocities are small. In the area where the velocities in the eddy are high, the error variance decreases. This reduction of errors is caused by numerical diffusion in the advection scheme. The effect of diffusion on the error covariance field is quite strong, partly because of the coarse resolution which is used. Note that it is not the pure error variance field which is advected, since the advection operator works separately on each of the covariance functions for the elements in the state vector. If higher resolution or a less diffusive advection scheme was used, this should give better results for the error propagation. The use of wider covariance functions would also decrease the diffusion. Figure 5 shows the error variance through the center of the domain in case 1A.

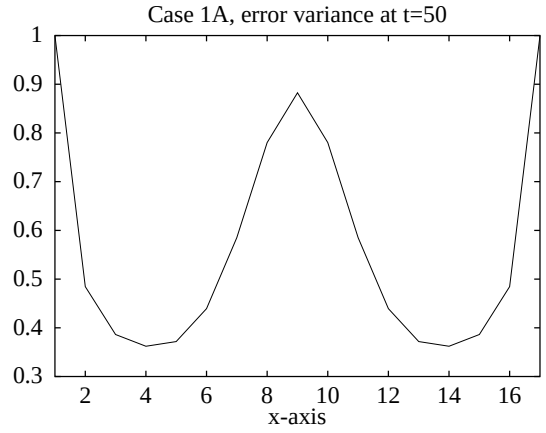

Fig. 5. The estimated error variance in layer one at the grid points $j = 9$ and $i = 1 \ldots 17$, at $t = 50$ for case 1A.

In case 1B the errors increase strongly at the locations where the eddy velocities are high. From the second term in (35) it can be seen that this effect requires a nonzero vorticity field, which is equivalent to requiring shear or curved

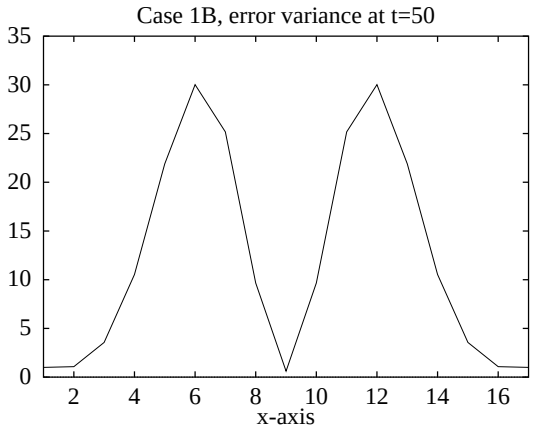

Fig. 6. The estimated error variance in layer one at the grid points $j = 9$ and $i = 1 \ldots 17$, at $t = 50$ for case 1B.

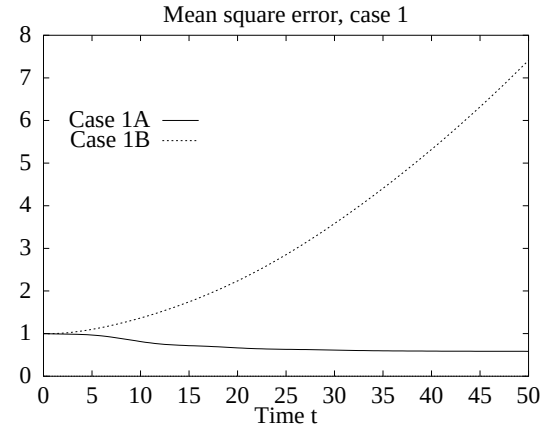

Fig. 7. The estimated mean square errors as a function of time for cases 1A and 1B.

flow. Thus, this instability may be interpreted as a shear flow instability for error covariance propagation. Figure 6 shows the error variance through the center of the domain in case 1B. Note the difference in scales in Figure 5 and 6.

In Figure 7 the mean square error is plotted, i.e. , the trace of the error covariance matrix divided by the number of grid points, in the two cases 1A and 1B. For case 1A the average error variance decreases in the beginning, since the most diffusive wavelengths are damped first. Thereafter the average error variance decreases more slowly with a much smaller effect of the diffusion. In case 1B the average error variance has an exponential growth. This result is actually quite pessimistic for the use of the extended Kalman filter with the QG model. It suggests the existence of an unbounded instability resulting from the linearization of the nonlinear error propagation equation. If the exact error propagation equation were solved, these instabilities would probably be saturated and damped, and this effect is lost through the linearization process. At this stage the following three approaches for handling this unbounded instability are proposed:

1. Using only the linear part of the transition matrix. This may work well if the estimated solution is close to the exact solution, and the errors are small. The contribution from the second term will then be small too. If this approach is used, the system noise should be increased to account for some of the error growth which is eliminated.

2. Controlling the instability with measurements. The instability is rather weak but will be exponential for long time integrations. If enough measurements are available, the errors will not be allowed to increase too much. Every time the errors in some domain are growing, the measurements will have increased influence in that domain, and the errors are reduced again.

3. Using higher order approximations for the error propagation equation. By using some higher order closure theory, which includes a damping or saturation term, it should be possible to control the instability. This must be done in an approximative way to be computationally affordable.

In this paper, only the first and second approach are discussed.

Data Assimilation Using the Extended Kalman Filter

Now some cases where measurements are assimilated using the extended Kalman filter are discussed. First a reference run is generated where the pure ocean model is integrated in time. A time series of the reference case is shown in Figure 8. The initial condition in the reference run is the same barotropic anticyclonic eddy which was used in case 1. The difference from case 1 is the introduction of a sloping bottom topography with linearly increasing depth in the y direction. This forces the eddy to propagate in the positive x direction along isolines of constant depth, and with a small component in the positive y direction. Behind the initial eddy a cyclonic eddy develops and after some time the eddies start to interact with the closed boundaries and each other.

The initial and system error variance is determined from the formulas (38) and (39). For the initial noise, $E_{\max} = 1.0$, and $E_{\min} = 0.01$, and for the system noise, $E_{\max} = 0.09$, and $E_{\min} = 0.01$.

Measurements are picked from the reference solution as stream function values at four different locations in layer one, (grid points $(1, 6, 6)$, $(1, 6, 12)$, $(1, 12, 6)$, $(1, 12, 12)$), with time intervals of $t = 2$. The measurements are perfect and no noise has been added. In the actual data assimilation runs the measurement error variance is set to $\sigma_o^2 = 0.05$, to reduce the weighting on the measurements. An eighth order Shapiro filter has been used every time step, as described by equations (36) and (37). The following two cases have been run:

Case 2A: Data assimilation experiment using only the first part of (35) for the error covariance propagation.

Case 2B: Data assimilation experiment using the full extended Kalman filter where both terms in (35) are used for the error covariance propagation.

In all experiments the initial stream function is set identically to zero. Figure 9 shows a time sequence of the stream function, the error variance field, and the potential vorticity for case 2A, and Figure 10 shows the same time sequence for case 2B. The structure of the stream function evolution is quite similar. The difference between the estimated stream functions and the reference stream function at $T = 60$ for case 2A and 2B, are shown in Figure 11. Table 2 gives the maximum norms and the average mean square errors in each layer for the same differences.

The simplified error covariance propagation used in case 2A performs better than the full extended Kalman filter. A reason for this may be the unbounded instabilities which

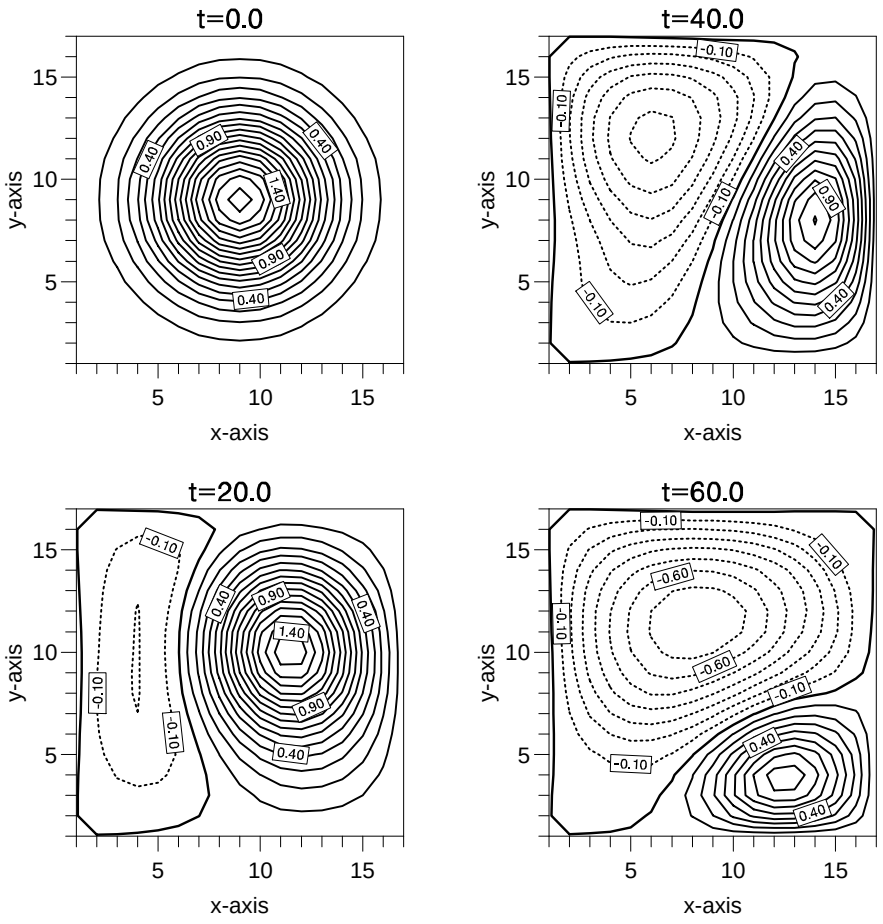

Fig. 8. Stream function for the reference case in the upper layer. The contour intervals are 0.1. The thick line is the zero-contour, the solid lines are positive contours, and the dashed lines are negative contours.

develop in case 2B. If the time series of the error variances for the two cases are compared (Figure 12), the difference is obvious. In case 2A the variances are decreasing steadily toward a minimum, just as in the one-dimensional example case. The errors are reduced every time measurements are assimilated, and the error increases between the assimilation times because of the system noise.

In case 2B it can be seen how the unbounded instabilities increase the average error, until measurements "kill" them, and the error is reduced again. When the errors are increasing because of these instabilities, the measurements will get too strong influence on the estimated solution in the areas with high errors. The strong error growth must be avoided if the extended Kalman filter shall give reliable results in a data assimilation scheme. Since the instabilities are localized to subdomains on the grid, very dense data coverage is required to prevent them from growing.

There is a significant difference between the exact values for mean square errors in Table 2 and the estimated mean square errors from Figure 12. This is caused by the use of incorrect system and measurement noise. The generation of measurements and the data assimilation experiments are using the same model. Since no artificial noise has been added, neither to the measurements nor the ocean model, both the system and measurement noise should be set to zero. In the examples, a nonzero variance is assumed both for the ocean model and the measurements for illustrational purposes. It also ensures numerical stability, since zero measurement and system noise results in zero error variance at the locations where the measurements are assimilated. This can lead to numerical instabilities if the error variance becomes negative owing to numerical truncation errors. The estimated error variance is therefore based on "incorrect" error statistics. Note that the influence of measurements is determined from

TABLE 2. Error Estimates

	Max. Error	MSE
Upper layer case 2A	0.15	0.0019
Lower layer case 2A	0.15	0.0033
Upper layer case 2B	0.27	0.0054
Lower layer case 2B	0.47	0.0166
Upper layer case 3A	1.50	0.1257
Lower layer case 3A	0.82	0.1343
Upper layer case 3B	0.26	0.0081
Lower layer case 3B	0.41	0.0221

The true errors in the estimated stream functions from cases 2 and 3 at $t = 60$. The first column contains the maximum error. The mean square error (MSE) is shown in the second column.

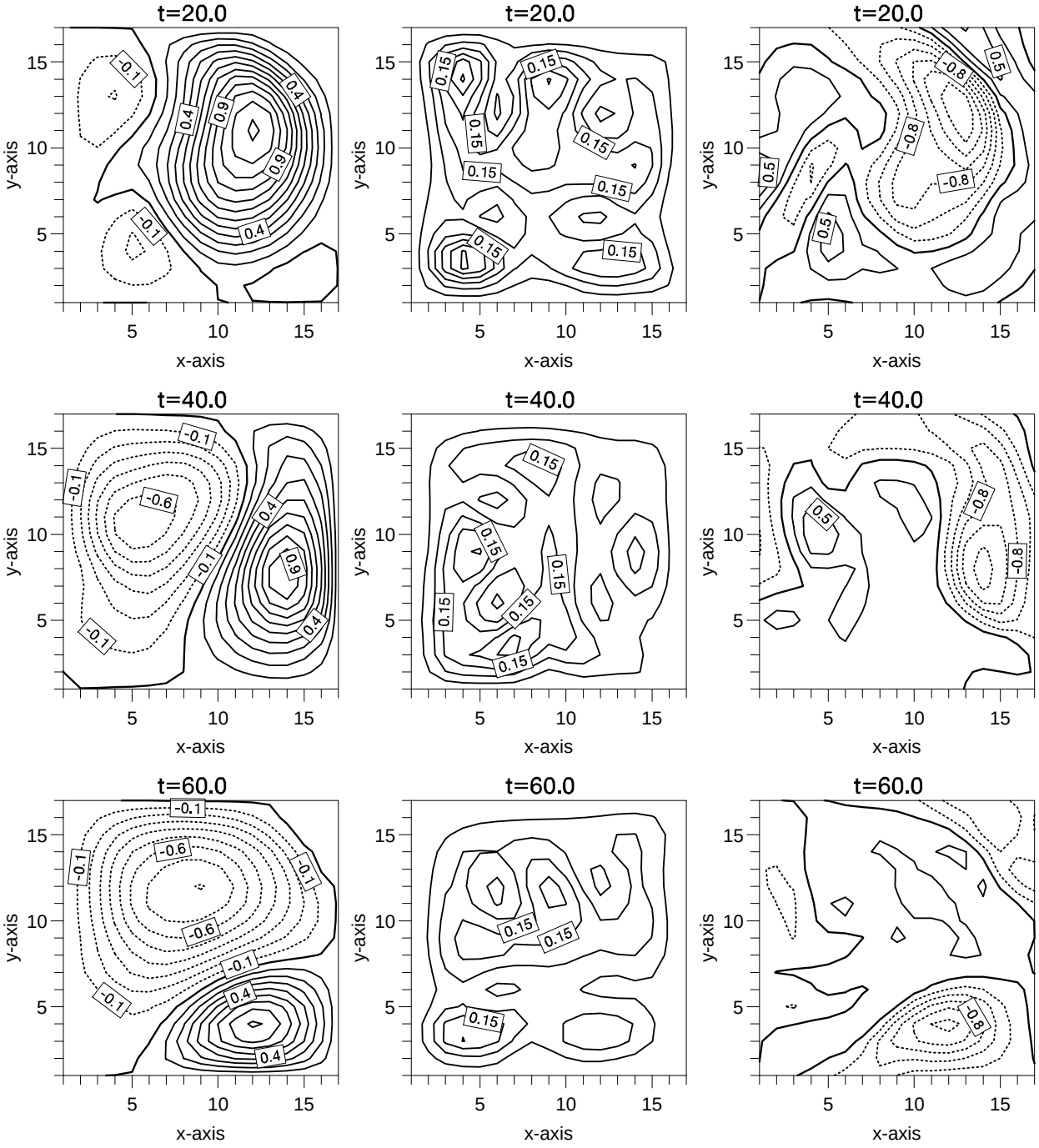

Fig. 9. Upper layer stream function (left column), error variance (middle column), and potential vorticity (right column) for case 2A. The contour intervals are 0.1 for the stream function, 0.05 for the error variances, and 0.25 for the potential vorticity field.

the relative magnitudes of the state, system and measurement variances. These variances should therefore be scaled properly, if they are used to estimate the exact state error variance. The covariance functions (not shown in a figure), will evolve dependent on the assimilation of measurements, the velocity field, and the error variance field. Their influence radii stay fairly constant (typically a few characteristic length scales), independent of the amplitude which is determined by the error variance field. The vorticity plots are discussed in connection with case 3.

Nonlinear Small-Scale Instabilities

The effect of nonlinear small-scale instabilities on the propagation of error covariances will now be illustrated, and the same parameters and example as in case 2B, with full error covariance propagation is used. The following modifications to case 2B are discussed.

Case 3A: Data assimilation experiment using the full extended Kalman filter, where no smoothing with the Shapiro filter (see appendix) has been applied neither for the stream function nor for the error covariances.

Case 3B: Data assimilation experiment using the full extended Kalman filter, where a Shapiro filter of $O(8)$ has

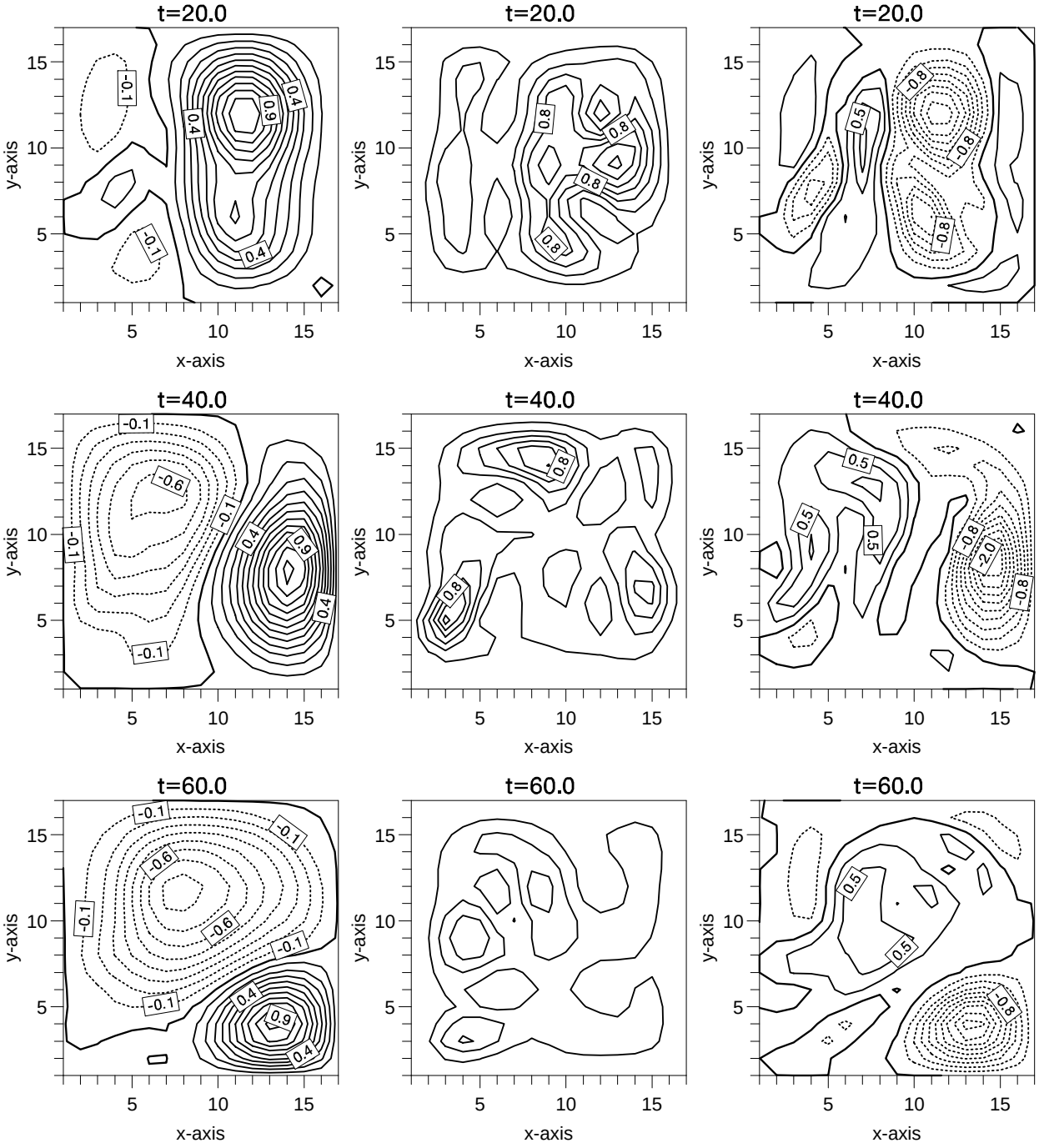

Fig. 10. Upper layer stream function (left column), error variance (middle column), and potential vorticity (right column) for case 2B. The contour intervals are 0.1 for the stream function, 0.2 for the error variances, and 0.25 for the potential vorticity field.

been applied every time step for the stream function, but not for the error covariance functions.

Figure 13 shows a time sequence of the stream function, the error variance field, and the potential vorticity for case 3A, where no Shapiro filter has been used. Figure 14 shows the same time sequence for case 3B, where the Shapiro filter has been used only for the stream function.

The effect of not using a filter to eliminate the small-scale noise is totally corrupting the results. In case 3A, instabilities occur both due to the noise in the stream function solution through the second term in (35), and also due to the nonlinear small-scale instabilities in the first term. The stream function solution is very bad with some additional structures which did not exist in the reference solution. The error variance field is completely different with several new structures and instabilities. The reason for this strong influence is that the second part of the transition matrix is proportional to the potential vorticity fields, where the oscillations in the stream function are amplified.

When using the Shapiro filter on the stream function in case 3B, the solution becomes much better, but it is still quite different from the results of case 2B (Figure 10), where the Shapiro filter was used both for the stream function and the error covariance matrix. The error variance field

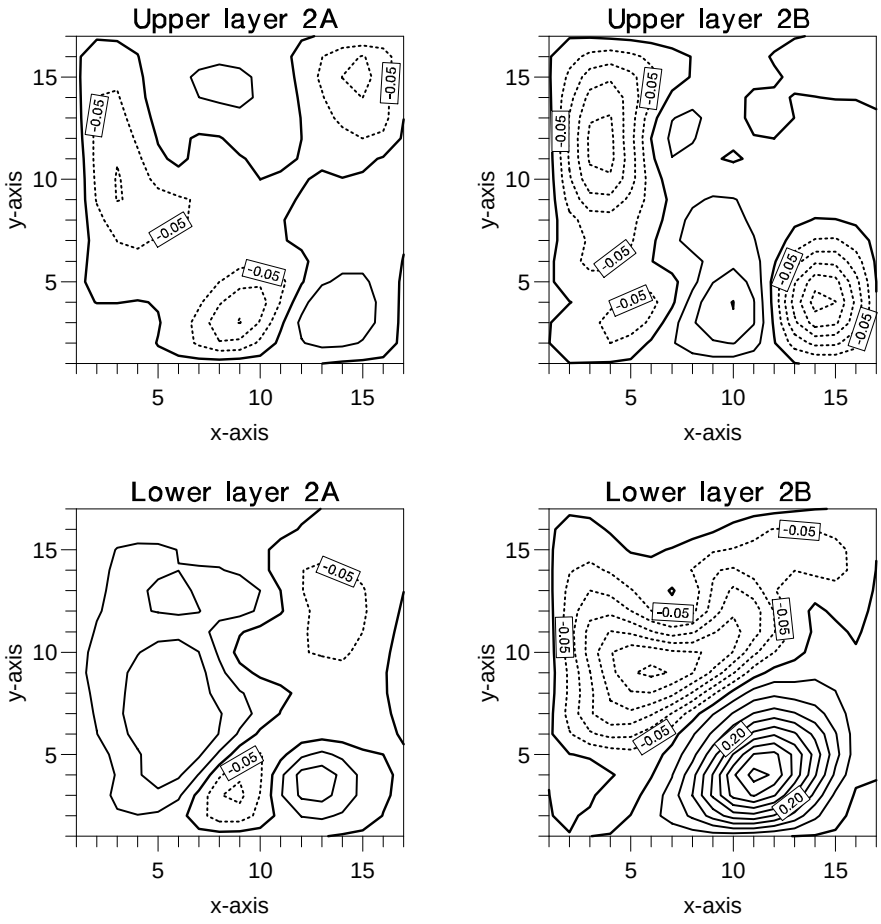

Fig. 11. The difference obtained when the stream function in cases 2A and 2B is subtracted from the exact reference solution for $t = 60$. The contour intervals are 0.05. In case 2A the errors are rather small, but in case 2B the amplitudes of both the cyclon and anticyclon are underestimated in layer 2.

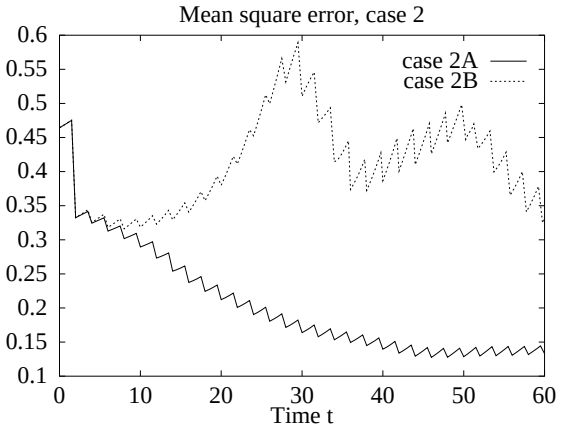

Fig. 12. The estimated mean square error as a function of time for cases 2A and 2B.

now looks more like the one from case 2B, but there are still some significant differences. The small-scale noise due to the pure advection term in (35) is still important, and they actually seem to trigger the more serious unbounded instability.

Since the error covariance evolution is directly dependent on the second term in equation (35), noise in the vorticity field will be reflected as noise in the covariance functions. The Kalman gain matrix (32) is proportional to the error covariance functions and it will also be affected by noise in them. The stream function will be influenced by noise in the Kalman gain matrix when equation (33) is used for assimilation of measurements. This coupling of the stream function and error covariance fields suggests that both the stream function and the error covariance functions should be filtered.

The importance of filtering the small-scale noise is clearly seen from the potential vorticity plots. In case 3A where no filtering has been applied neither for the stream function nor the error covariance functions, the potential vorticity field becomes extremely noisy (Figure 13). When the stream function is smoothed in case 3B, the most significant noise is removed and the vorticity field appears to be quite realistic (Figure 14). The effect of filtering the error covariance functions is seen by comparing the vorticity fields for case 2B and case 3B in Figures 10 and 14. It provides a smoother vorticity field, since the noise in the error covari-

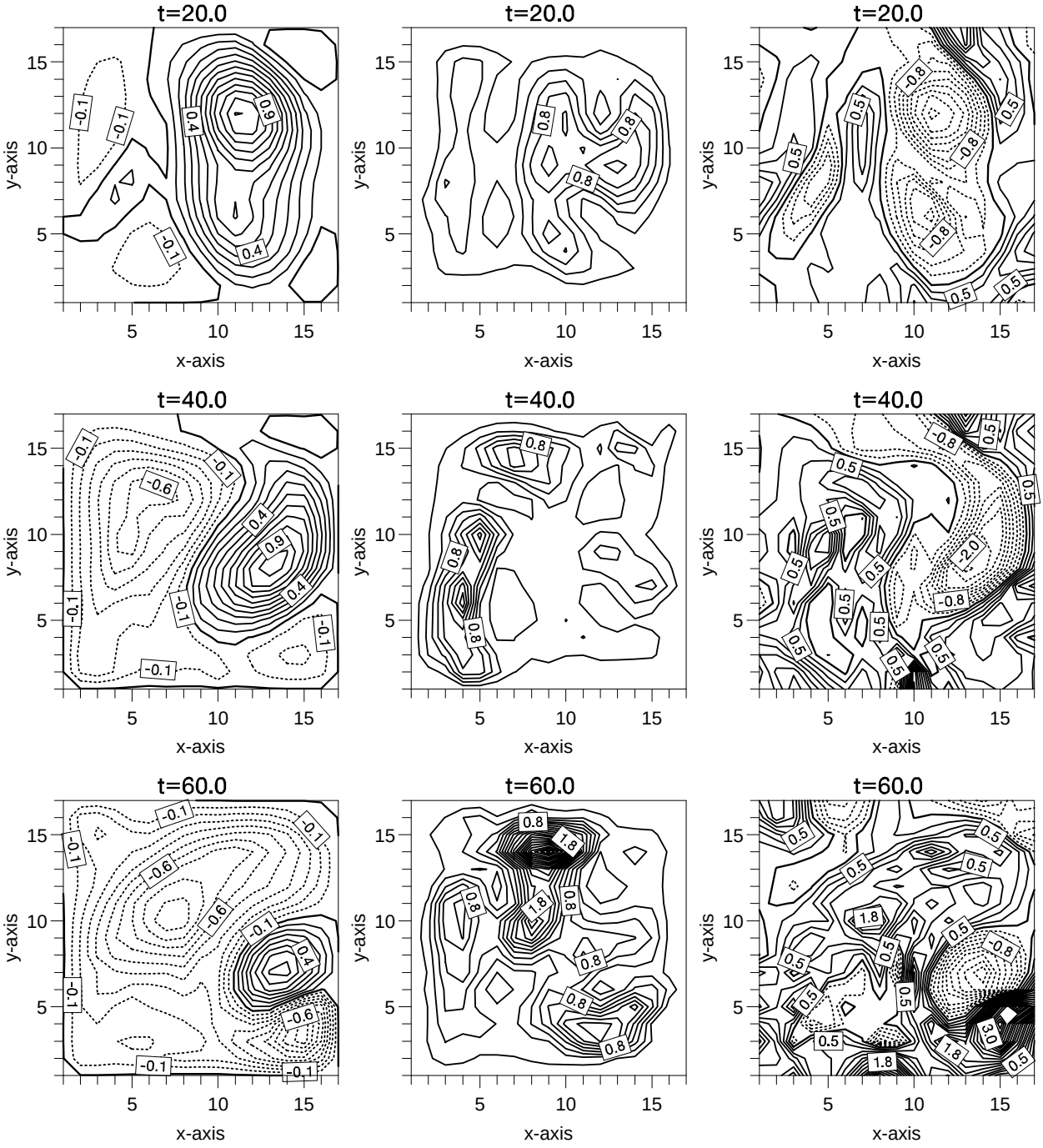

Fig. 13. Upper layer stream function (left column), error variance (middle column), and potential vorticity (right column) for case 3A. The contour intervals are 0.1 for the stream function, 0.2 for the error variances, and 0.25 for the potential vorticity field. The Shapiro filter has not been used, for either the stream function or the error covariance matrix.

ance functions no longer affects the stream function field when measurements are assimilated, using equation (33).

A conclusion from the data assimilation experiment is that case 2A, using only the first part of (35) for error covariance evolution, and where both the stream function and the error covariance functions are smoothed, gives the solution which is closest to the reference solution at $t = 60$.

Conclusions and Discussion

The formulation of the extended Kalman filter with a nonlinear multilayer quasi-geostrophic ocean circulation model has been discussed, including the nonlinear effects on the error covariance propagation, like the unbounded instability caused by the linearization of the error covariance propagation equation. A multilayer ocean model have been used, even if this reduces the horizontal resolution which is possible on existing computers. The main reason for this is that the baroclinic instabilities should be included in most mesoscale simulations to give reasonably good results. No verification of the validity of the approximative error covariance propagation equation has been given, and this is an important subject which requires further study.

The transition matrix can be expressed as two parts,

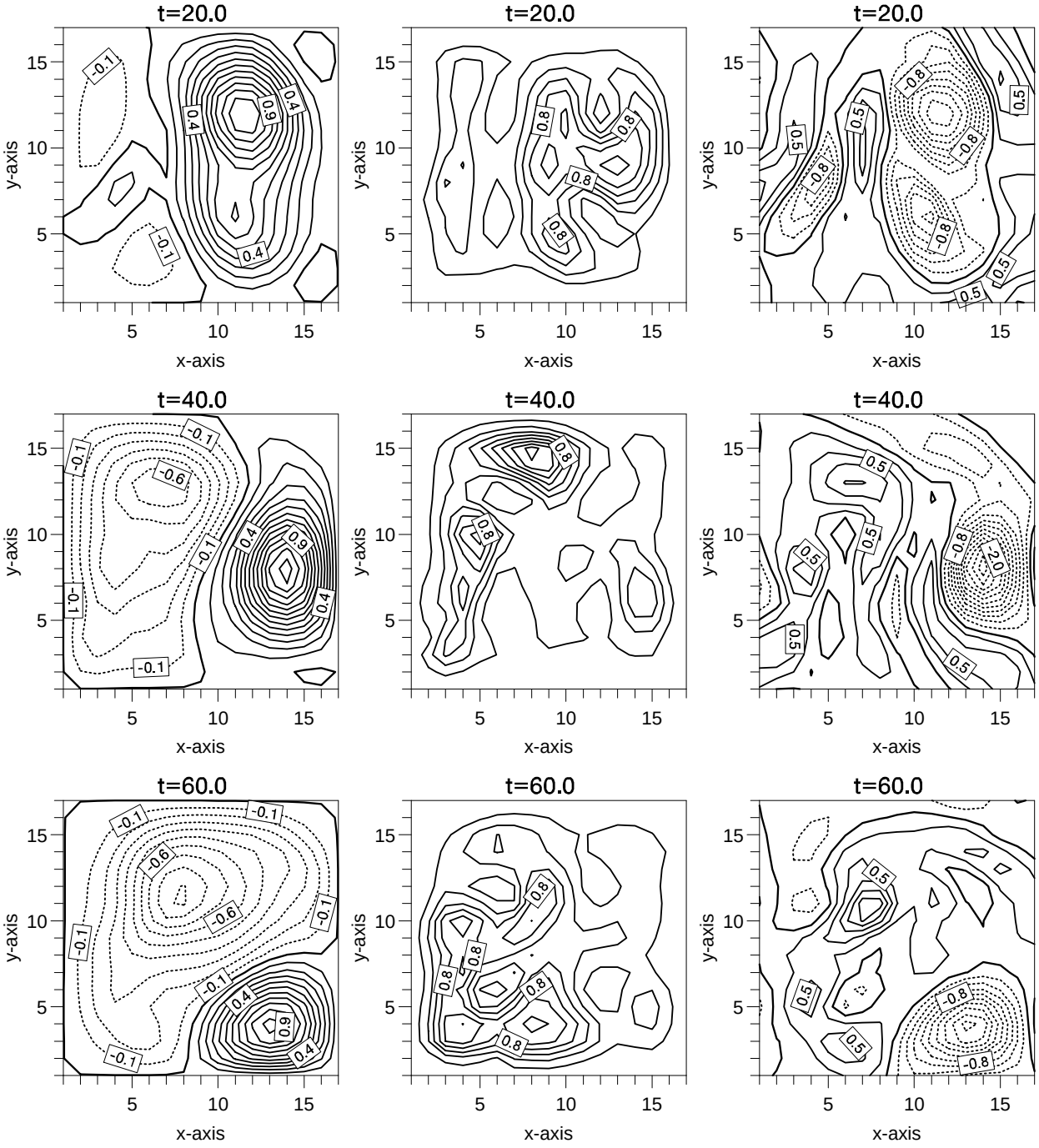

Fig. 14. Upper layer stream function (left column), error variance (middle column), and potential vorticity (right column) for case 3B. The contour intervals are 0.1 for the stream function, 0.2 for the error variances, and 0.25 for the potential vorticity field. The Shapiro filter has been used for the stream function but not for the error covariance matrix.

where one part contains pure evolution due to the model velocity field, and the second part is the statistical correction term resulting from the nonlinearity in the error propagation equation. This makes it possible to test the data assimilation scheme both with and without the statistical correction, and to totally remove the unbounded instability connected to it.

The unbounded instability has actually proven to be rather strong for the QG model. If the full extended Kalman filter shall be used, it requires either an extensive data coverage which is able to control the instability, or some higher order closure equations which introduce damping of the instability. The inclusion of higher moments in the approximative error propagation equation will make the Kalman filter very computationally expensive, and an approximative method should be used.

Fortunately, pure error covariance evolution in the model velocity field has given quite good results in our cases. It also has some other advantages which should be taken into account. The coding is very simple, and the existing routines in the ocean model can be used with only slight modifications. This simplified propagation is probably the best that can be done without the inclusion of equations which damp the unbounded instability. It contains error propa-

gation based on the estimated state, and if the estimate is close to the exact solution it should perform very well.

With good knowledge of the error statistics, both for the dynamical model and the measurements, the inclusion of error covariance propagation should certainly improve the estimate. An important issue will be to examine if the extended Kalman filter, with some version of the error propagation equation, gives good enough results compared to optimal interpolation (OI), to defend the considerably greater computational cost.

Data assimilation using the extended Kalman filter in realistic ocean circulation models requires super computers with large memory and extremely fast CPUs. The computational load has been used as an argument against the use of the Kalman filter in data assimilation, and most of the research has so far been focused on adjoint methods, nudging, and OI. Fortunately, computers are becoming more powerful, and there are now super computers available which can handle data assimilation using the extended Kalman filter with a QG model for reasonably large grids. The error covariance propagation equation is also very well suited to be computed on the massive parallel computers like the MasPar 1200 series and the Connection Machines (CM2). The examples have been run on a Cray X-MP, and each case required about 20 min of CPU.

APPENDIX

The Time Step Scheme

Since the transition matrix F_k' from (26) is strongly dependent on the choice of advection scheme, it is important to find a convenient scheme for the advection of vorticity, which also implies a simple transition matrix with as few bands as possible. The following criteria have been used to choose the scheme:

1. The scheme should be explicit to avoid the solution of extra systems of equations when updating the error covariance matrix.

2. It should only reference function values at the points in the square $[i-1:i+1, j-1:j+1]$ to minimize the number of bands in the transition matrix.

3. The scheme should have high accuracy for smooth flow.

4. It should be stable for as large time steps as possible.

5. As has been pointed out in the text, it should be a one-step scheme in time.

Here a short discussion of the advection scheme which has been used in the ocean model is given. A Taylor expansion of the vorticity $\zeta(x_i, y_j, t)$ in time about the point (x_i, y_j, t_k) denoted by subscript 0, gives

$$\begin{aligned}
&\zeta(x_i, y_j, t+\Delta t) = \zeta_0 \\
&- \left\{ u_0 + \frac{\Delta t}{2}\left(\left.\frac{\partial u}{\partial t}\right|_0 - u_0 \left.\frac{\partial u}{\partial x}\right|_0 - v_0 \left.\frac{\partial u}{\partial y}\right|_0 \right) \right\} \Delta t \left.\frac{\partial \zeta}{\partial x}\right|_0 \\
&- \left\{ v_0 + \frac{\Delta t}{2}\left(\left.\frac{\partial v}{\partial t}\right|_0 - u_0 \left.\frac{\partial v}{\partial x}\right|_0 - v_0 \left.\frac{\partial v}{\partial y}\right|_0 \right) \right\} \Delta t \left.\frac{\partial \zeta}{\partial y}\right|_0 \\
&+ \left.\frac{u^2 \Delta t^2}{2} \frac{\partial^2 \zeta}{\partial x^2}\right|_0 + uv\Delta t^2 \left.\frac{\partial^2 \zeta}{\partial x \partial y}\right|_0 + \left.\frac{v^2 \Delta t^2}{2} \frac{\partial^2 \zeta}{\partial y^2}\right|_0 \\
&+ O((u\Delta t)^3; (v\Delta t)^3), \qquad (40)
\end{aligned}$$

where the advection equation (9) has been substituted for the temporal derivatives.

When the velocity field is dependent on both space and time, the velocities are estimated at the point

$$(x_i - \tfrac{1}{2}u_0\Delta t, y_j - \tfrac{1}{2}v_0\Delta t, t_k + \tfrac{1}{2}\Delta t) \qquad (41)$$

by a first-order Taylor expansion. This is the midpoint between the point (x_i, y_j, t_{k+1}), which is to be updated, and the point

$$(x', y', t_k) = (x_i - u\Delta t, y_j - v\Delta t, t_k), \qquad (42)$$

which is an estimate of the point containing the vorticity at time t_k, which is conserved when it moves along the fluid path into (x_i, y_j) at time t_{k+1}.

First a scheme is developed and discussed in the linear case when the velocities are constant in time and space. When defining

$$\alpha = \frac{u\Delta t}{\Delta x} \quad \text{and} \quad \beta = \frac{v\Delta t}{\Delta x}, \qquad (43)$$

and using a second-order centered approximation for the spatial derivatives, a "general" scheme may be written as

$$\begin{aligned}
\zeta_{i,j}^{k+1} &= \zeta_{i,j}^k \\
&-\frac{1}{2}\alpha\left(\frac{1-s}{2}(\zeta_{i+1,j+1}^k - \zeta_{i-1,j+1}^k) + s(\zeta_{i+1,j}^k - \zeta_{i-1,j}^k)\right. \\
&\qquad \left. + \frac{1-s}{2}(\zeta_{i+1,j-1}^k - \zeta_{i-1,j-1}^k)\right) \\
&-\frac{1}{2}\beta\left(\frac{1-s}{2}(\zeta_{i+1,j+1}^k - \zeta_{i+1,j-1}^k) + s(\zeta_{i,j+1}^k - \zeta_{i,j-1}^k)\right. \\
&\qquad \left. + \frac{1-s}{2}(\zeta_{i-1,j+1}^k - \zeta_{i-1,j-1}^k)\right) \\
&+\frac{1}{2}\alpha^2(\zeta_{i+1,j}^k - 2\zeta_{i,j}^k + \zeta_{i-1,j}^k) \\
&+\frac{1}{2}\beta^2(\zeta_{i,j+1}^k - 2\zeta_{i,j}^k + \zeta_{i,j-1}^k) \\
&+\frac{1}{4}\alpha\beta(\zeta_{i+1,j+1}^k - \zeta_{i+1,j-1}^k - \zeta_{i-1,j+1}^k + \zeta_{i-1,j-1}^k) \\
&+O((\alpha\Delta x)^3; (\beta\Delta y)^3). \qquad (44)
\end{aligned}$$

In this formula $s = 1$ is the standard case where the first derivatives are calculated from points on a line and therefore do not include any information of the two-dimensionality of the field. For values of $s \neq 1$ the first derivatives are calculated by some averaging of the derivatives on a plane, as discussed by *Smolarkiewicz* [1982].

The Linear Stability of the Advection Scheme

The linear stability and accuracy of this scheme are examined by assuming a solution on the form $\zeta = e^{i(\omega t - \kappa x - \mu y)}$, where the frequency is allowed to be complex $\omega = \omega_r + i\omega_i$, which results in the wave

$$\zeta = e^{-\omega_i t} e^{i(\omega_r t - \kappa x - \mu y)}. \qquad (45)$$

This is substituted in the scheme (44) and the nondimensional variables

$$\theta_x = \frac{\kappa\Delta x}{\pi}, \quad \theta_y = \frac{\mu\Delta y}{\pi}, \quad \omega' = \frac{\omega\Delta t}{\pi}. \qquad (46)$$

are defined. This results in the two equations

$$e^{-\pi\omega_i'} \cos \pi\omega_r' = \mathrm{Re}(\lambda) \qquad (47)$$

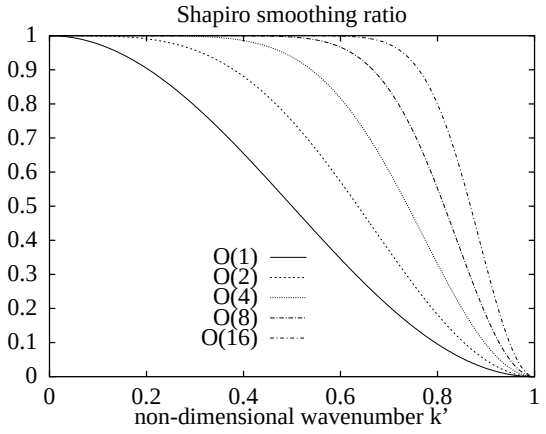

Fig. 15. The amplitude damping ratios for different orders of the Shapiro filter, as a function of non-dimensional wave numbers $k' = (k\Delta x)/\pi$. Here, $k' = 1$ corresponds to waves with wavelength $\lambda = 2\Delta x$ and $k' = 0$ is infinitively long waves.

and

$$e^{-\pi\omega_i'} \sin \pi\omega_r' = \mathrm{Im}(\lambda), \tag{48}$$

where λ is given by

$$\begin{aligned}\lambda = 1 &- \alpha^2(1 - \cos\pi\theta_x) - \beta^2(1 - \cos\pi\theta_y) \\ &- \alpha\beta \sin\pi\theta_x \sin\pi\theta_y \\ &+ i[\alpha \sin\pi\theta_x(s + (1-s)\cos\pi\theta_y) \\ &+ \beta \sin\pi\theta_y(s + (1-s)\cos\pi\theta_x)].\end{aligned} \tag{49}$$

Solving for ω_i' and ω_r' from (47) and (48) results in the two equations

$$(e^{-\pi\omega_i'})^2 = \mathrm{Re}(\lambda)^2 + \mathrm{Im}(\lambda)^2 \tag{50}$$

and

$$\omega_r' = \frac{1}{\pi} \arctan \frac{\mathrm{Im}(\lambda)}{\mathrm{Re}(\lambda)}. \tag{51}$$

From (45), stability is ensured if $\omega_i' \geq 0$, which from (50) is equivalent to the condition $\mathrm{Re}(\lambda)^2 + \mathrm{Im}(\lambda)^2 \leq 1$ The accuracy of the scheme is given by the dispersion relation (51). These schemes are discussed by *Smolarkiewicz* [1982], and he suggested the use of $s = 0.5$, which results in a scheme which is stable under the condition

$$(\alpha^2 + \beta^2)^{1/2} \leq 1, \tag{52}$$

which is a great improvement from the standard case with $s = 1$, which is stable when

$$(\alpha^2 + \beta^2)^{1/2} \leq 0.5. \tag{53}$$

The Nonlinear Case

The proposed scheme satisfies the first four conditions, but because the time derivatives of the velocities occur in the scheme (40), information from a minimum of two time levels is needed. With the assumption of a slowly varying velocity field in time, nondimensional $\partial(u,v)/\partial t \ll \partial(u,v)/\partial x, \partial(u,v)/\partial y$, the time derivatives may be neglected. That results in a scheme which is second order in Δx and Δy, and it is second order in Δt if the velocity field really is slowly varying in time; if not, it is first order in Δt.

In this paper the discretized scheme (44) is used with $s = 0.5$ and velocities calculated from

$$u = u_0 - \tfrac{1}{2}u_0\Delta t \left.\frac{\partial u}{\partial x}\right|_0 - \tfrac{1}{2}v_0\Delta t \left.\frac{\partial u}{\partial y}\right|_0, \tag{54}$$

$$v = v_0 - \tfrac{1}{2}u_0\Delta t \left.\frac{\partial v}{\partial x}\right|_0 - \tfrac{1}{2}v_0\Delta t \left.\frac{\partial v}{\partial y}\right|_0. \tag{55}$$

Nonlinear Instability

Energy is accumulated at high wave numbers (wavelengths of order $O(2\Delta x)$), and has to be removed. The Shapiro filter (which is developed and discussed in *Shapiro* [1970]) has the properties that it totally removes the waves with wavenumber $2\Delta x$, and at the same time it restores infinitely long waves to their original value. A plot of the amplitude reduction factor for different orders of the Shapiro filter, as a function of nondimensional wavenumbers is shown in Figure 15. A simple general formula for the one-dimensional filter was given by *Smolarkiewicz* [1982]. Unfortunately, his formula contained a typing error, and we therefore give the correct formula for a one-dimensional filter of order n as

$$\Psi_i^{\mathrm{filt}} = \Psi_i + \frac{(-1)^{n-1}}{2^{2n}} \sum_{j=0}^{2n} \frac{(-1)^j (2n)!}{j!(2n-j)!} \Psi_{i+n-j}. \tag{56}$$

In this expression, index i corresponds to the grid point to be updated, j is a counter running over the grid points which are used in the updating of grid point i. Note that the operator (56) is symmetrical. It seems that the Shapiro filter of some order is the optimal smoothing and filtering technique for removing nonlinear small-scale instabilities without destroying the physics in the model. A recent review on recursive and implicit filters has been given by *Raymond and Garder* [1991].

When filtering data on a two-dimensional grid, the one-dimensional operator (56) can be used first for all the rows in the x direction, and thereafter for all the columns in the y direction.

It has been chosen not to update the boundary points with the Shapiro filter. When updating grid points close to the boundaries, the operator (56) will reference points outside the boundary. The existence of fictive grid points located outside the boundary, with values which are symmetrical about the value of the boundary point, is assumed. That is, the value of the ith fictive point outside the boundary will have the value given by a straight line through the value of the boundary point and the value of the ith point inside the boundary. By using these in the Shapiro filter close to the boundaries, boundary effects are avoided.

Acknowledgments. The author would like to thank P. M. Haugan and A. F. Bennett for valuable comments and suggestions. The work was supported by the Norwegian Research Council for Science and the Humanities.

REFERENCES

Anderson, B. D. O., and J. B. Moore, *Optimal Filtering, Inform. and Syst. Sci. Ser.*, Prentice-Hall, Englewood Cliffs, N. J., 1979.

Bennett, A. F., and W. P. Budgell, Ocean data assimilation and the Kalman filter: Spatial regularity, *J. Phys. Oceanogr.*,

17(10), 1583–1601, 1987.

Bennett, A. F., and W. P. Budgell, The Kalman smoother for a linear quasigeostrophic model of ocean circulation, *Dyn. Atmos. Oceans*, *13*(3-4), 219–267, 1989.

Bierman, G. J., *Factorization Methods for Discrete Sequential Estimation*, *Math. in Sci. and Eng.*, vol. 128, Academic, San Diego, Calif., 1977.

Budgell, W. P., Nonlinear data assimilation for shallow water equations in branched channels, *J. Geophys. Res.*, *91*(C9), 10,633–10,644, 1986.

Budgell, W. P., Stochastic filtering of linear shallow water wave processes, *SIAM J. Sci. Stat. Comput.*, *8*(2), 152–170, 1987.

Chao, S.-Y., Bimodality of the Kuroshio, *J. Phys. Oceanogr.*, *14*, 92–103, 1984.

Charney, J. G., R. Fjørtoft, and J. von Neuman, Numerical integration of the barotropic vorticity equation, *Tellus*, *2*(4), 237–254, 1950.

Cohn, S. E., and D. F. Parrish, The behavior of forecast error covariances for a Kalman filter in two dimensions, *Mon. Weather Rev.*, *119*, 1757–1785, 1991.

Courtier, P., and O. Talagrand, Variational assimilation of meteorological observations with the adjoint vorticity equation, II, Numerical results, *Q. J. R. Meteorol. Soc.*, *113*, 1329–1347, 1987.

Courtier, P., and O. Talagrand, Variational assimilation of meteorological observations with the direct and adjoint shallow-water equations, *Tellus*, *42A*(5), 531–549, 1990.

Dee, D. P., Simplification of the Kalman filter for meteorological data assimilation, *Q. J. R. Meteorol. Soc.*, *117*, 365–384, 1991.

Gelb, A., *Applied Optimal Estimation*, MIT Press, Cambridge, Mass., 1974.

Ghil, M., Meteorological data assimilation for oceanographers, Part I, Description and theoretical framework, *Dyn. Atmos. Oceans*, *13*(3-4), 171–218, 1989.

Ghil, M., and P. Malanotte-Rizzoli, Data assimilation in meteorology and oceanography, *Adv. Geophys.*, *33*, 141–266, 1991.

Ghil, M., S. Cohn, J. Tavantzis, K. Bube, and E. Isaacson, Applications of estimation theory to numerical weather prediction, in *Dynamic Meteorology: Data Assimilation Methods*, edited by L. Bengtsson, M. Ghil, and E. Kallén, pp. 139–224, Springer Verlag, New York, 1981.

Haugan, P. M., G. Evensen, J. A. Johannessen, O. M. Johannessen, and L. Pettersson, Modeled and observed mesoscale circulation and wave-current refraction during the 1988 Norwegian continental shelf experiment, *J. Geophys. Res.*, *96*(C6), 10,487–10,506, 1991.

Holland, W. R., The role of mesoscale eddies in the general circulation of the ocean—Numerical experiments using a wind-driven quasi-geostrophic model, *J. Phys. Oceanogr.*, *8*, 363–392, 1978.

Ikeda, M., Meanders and detached eddies of a strong eastward-flowing jet using a two-layer quasi-geostrophic model, *J. Phys. Oceanogr.*, *11*, 526–540, 1981.

Ikeda, M., and J. R. Apel, Mesoscale eddies detached from spatially growing meanders in an eastward-flowing oceanic jet using a two-layer quasi-geostrophic model, *J. Phys. Oceanogr.*, *11*, 1638–1661, 1981.

Ikeda, M., J. A. Johannessen, K. Lygre, and S. Sandven, A process study of mesoscale meanders and eddies in the Norwegian coastal current, *J. Phys. Oceanogr.*, *19*, 20–35, 1989.

Jazwinski, A. H., *Stochastic Processes and Filtering Theory*, Academic, San Diego, Calif., 1970.

Lacarra, J.-F., and O. Talagrand, Short-range evolution of small perturbations in a barotropic model, *Tellus*, *40A*(2), 81–95, 1988.

Lewis, J. M., and J. C. Derber, The use of adjoint equations to solve a variational adjustment problem with advective constraints, *Tellus*, *37A*(4), 309–322, 1985.

Long, R. B., and W. C. Thacker, Data assimilation into a numerical equatorial ocean model, I, The model and the assimilation algorithm, *Dyn. Atmos. Oceans*, *13*(3-4), 379–412, 1989*a*.

Long, R. B., and W. C. Thacker, Data assimilation into a numerical equatorial ocean model, II, Assimilation experiments, *Dyn. Atmos. Oceans*, *13*(3-4), 413–439, 1989*b*.

Lorenz, E. N., Deterministic nonperiodic flow, *J. Atmos. Sci.*, *20*, 130–141, 1963.

Miller, R. N., Toward the application of the Kalman filter to regional open ocean modeling, *J. Phys. Oceanogr.*, *16*, 72–86, 1986.

Miller, R. N., Tropical data assimilation experiments with simulated data: The impact of the tropical ocean and global atmosphere thermal array for the ocean, *J. Geophys. Res.*, *95*(C7), 11,461–11,482, 1990.

Miller, R. N., and A. F. Bennett, Numerical simulation of flows with locally characteristic boundaries, *Tellus*, *40A*(4), 303–323, 1988.

Miller, R. N., and M. A. Cane, A Kalman filter analyses of sea level height in the tropical Pacific, *J. Phys. Oceanogr.*, *19*, 773–790, 1989.

Miller, R. N., and M. Ghil, Data assimilation in strongly nonlinear current systems, Paper presented at the International Symposium on Data Assimilation of Observations in Meteorology and Oceanography, World Meteorological Organization, Clermont-Ferrand France, July, 9–13, 1990.

Pedlosky, J., *Geophysical Fluid Dynamics*, 2nd edition, Springer–Verlag, New York, 1987.

Raymond, W. H., and A. Garder, A review of recursive and implicit filters, *Mon. Weather Rev.*, *119*, 477–495, 1991.

Rienecker, M. M., and R. N. Miller, Ocean data assimilation using optimal interpolation with a quasi-geostrophic model, *J. Geophys. Res.*, *96*(C8), 15,093–15,103, 1991.

Shapiro, R., Smoothing, filtering, and boundary effects, *Rev. Geophys.*, *8*(2), 359–387, 1970.

Smolarkiewicz, P. K., The multi-dimensional Crowley advection scheme, *Mon. Weather Rev.*, *110*, 1968–1983, 1982.

Stengel, R. F., *Stochastic Optimal Control, Theory And Application*, John Wiley, New York, 1986.

Sweet, R. A., A cyclic reduction algorithm for solving block tridiagonal systems of arbitrary dimension, *SIAM J. Numer. Anal.*, *14*(4), 706–720, 1977.

Talagrand, O., and P. Courtier, Variational assimilation of meteorological observations with the adjoint vorticity equation, I, Theory, *Q. J. R. Meteorol. Soc.*, *113*, 1311–1328, 1987.

Thacker, W. C., Fitting models to inadequate data by enforcing spatial and temporal smoothness, *J. Geophys. Res.*, *93*(C9), 10,655–10,665, 1988.

Thacker, W. C., and R. B. Long, Fitting dynamics to data, *J. Geophys. Res.*, *93*(C2), 1227–1240, 1988.

Tzafestas, S. G., Distributed parameter state estimation, in *Distributed Parameter Systems: Identification, Estimation and Control*, edited by W. H. Ray and D. G. Lainiotis, pp. 135–208, Marcel Dekker, New York, 1978.

G. Evensen, Nansen Environmental and Remote Sensing Center, Edvard Griegsvei 3a, N–5037 Solheimsviken/Bergen, Norway.

(Received January 22, 1992;
revised July 21, 1992;
accepted July 27, 1992.)